7-20-2020

The Mechanosensitive Ion Channel MSL10 Potentiates Responses to Cell Swelling in Arabidopsis Seedlings

Debarati Basu
Washington University in St. Louis

Elizabeth S. Haswell
Washington University in St. Louis

Article

Current Biology

The Mechanosensitive Ion Channel MSL10 Potentiates Responses to Cell Swelling in *Arabidopsis* Seedlings

Graphical Abstract

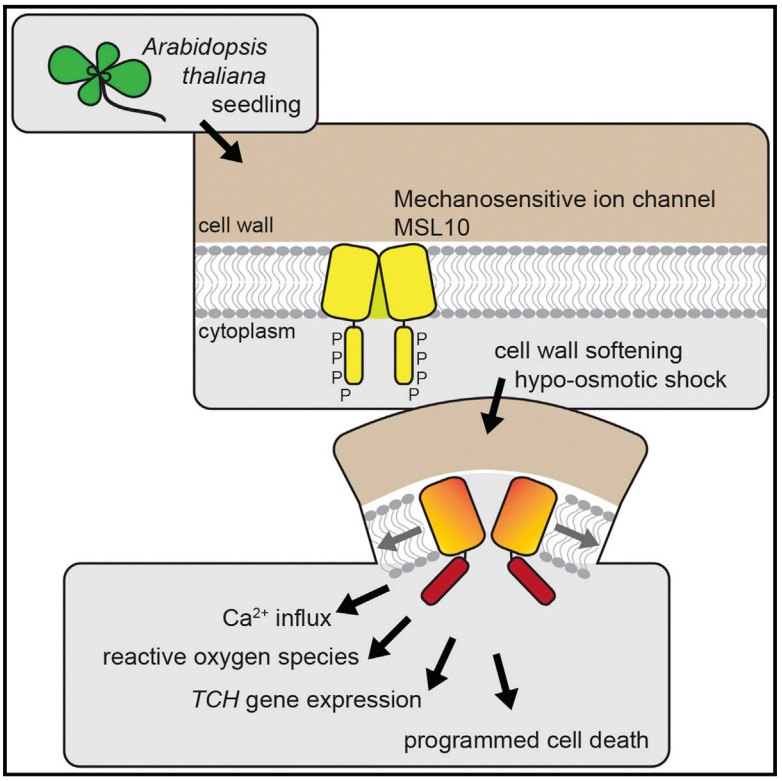

Authors

Debarati Basu, Elizabeth S. Haswell

Correspondence

ehaswell@wustl.edu

In Brief

Haswell and Basu use a seedling-based cell swelling assay in *Arabidopsis thaliana* to show that the mechanosensitive ion channel MscS-like 10 is required for several known hypo-osmotic shock responses. Furthermore, cell swelling induces programmed cell death in a manner that requires MSL10 and is regulated by phosphorylation of its N terminus.

Highlights

- A cell swelling assay in *Arabidopsis thaliana* seedlings was developed
- Cell swelling induced multiple responses, including programmed cell death (PCD)
- The mechanosensitive ion channel MSL10 potentiated all of these responses
- A phosphomimetic MSL10 variant was unable to potentiate cell swelling-induced PCD

Basu & Haswell, 2020, Current Biology *30*, 2716–2728
July 20, 2020
https://doi.org/10.1016/j.cub.2020.05.015

CellPress

CellPress

Current Biology

Article

The Mechanosensitive Ion Channel MSL10 Potentiates Responses to Cell Swelling in *Arabidopsis* Seedlings

Debarati Basu[1] and Elizabeth S. Haswell[1,2,3,*]
[1]NSF Center for Engineering Mechanobiology, Department of Biology, Washington University in St. Louis, St. Louis, MO 63130, USA
[2]Twitter: @ehaswell
[3]Lead Contact
*Correspondence: ehaswell@wustl.edu
https://doi.org/10.1016/j.cub.2020.05.015

SUMMARY

The ability to respond to unanticipated increases in volume is a fundamental property of cells, essential for cellular integrity in the face of osmotic challenges. Plants must manage cell swelling during flooding, rehydration, and pathogen invasion—but little is known about the mechanisms by which this occurs. It has been proposed that plant cells could sense and respond to cell swelling through the action of mechanosensitive ion channels. Here, we characterize a new assay to study the effects of cell swelling on *Arabidopsis thaliana* seedlings and to test the contributions of the mechanosensitive ion channel MscS-like10 (MSL10). The assay incorporates both cell wall softening and hypo-osmotic treatment to induce cell swelling. We show that MSL10 is required for several previously demonstrated responses to hypo-osmotic shock, including a cytoplasmic calcium transient within the first few seconds, accumulation of ROS within the first 30 min, and increased transcript levels of mechano-inducible genes within 60 min. We also show that cell swelling induces programmed cell death within 3 h in a MSL10-dependent manner. Finally, we show that MSL10 is unable to potentiate cell swelling-induced death when phosphomimetic residues are introduced into its soluble N terminus. Thus, MSL10 functions as a phospho-regulated membrane-based sensor that connects the perception of cell swelling to a downstream signaling cascade and programmed cell death.

INTRODUCTION

Cells from all organisms must actively maintain an optimal volume; left uncontrolled, the passive diffusion of water into the cell would lead to extreme swelling and loss of integrity [1–3]. In plants, cell volume regulation is required to maintain cell shape, accomplish cell expansion and growth, drive cellular movements like stomatal opening, and prevent wilting [4, 5]. Plant cells may swell in the early stages of flooding, upon rehydration after desiccation, during water soaking induced by pathogen, or in response to cell wall damage by pathogens [6–8]. In the laboratory, cell swelling is induced by subjecting tissues, cell suspensions, or protoplasts to sudden large drops in media osmolarity or by disrupting the microtubule cytoskeleton (e.g., [9, 10]).

There are both immediate and delayed responses to such cell swelling. A transient increase in cytoplasmic calcium ($[Ca^{2+}]_{cyt}$) in response to hypo-osmotic shock has been documented in cultured tobacco, rice and *Arabidopsis* cells [11–19], *Arabidopsis* leaves [20], and *Arabidopsis* root tips [21]. Hypo-osmotic shock also produces a burst of reactive oxygen species (ROS) [22–24] and leads to the activation of mitogen-activated kinases [10, 12, 25] and other stress responses [26–29]. In *Arabidopsis*, a number of mechano- and Ca^{2+}-responsive genes are induced in root tips after hypo-osmotic treatment [21]. A family of bZIP transcription factors is translocated to the nucleus upon hypo-osmotic shock, where they are thought to upregulate rehydration-responsive genes [27, 30, 31]. Despite these many observations, it is still not clear how these downstream signaling components are connected or how they might lead to adaptive responses.

It is also poorly understood how cell swelling is initially perceived in plants. The many potential signals include molecular crowding, membrane tension, osmotic gradient, turgor, membrane curvature, cell wall damage, and the disruption of the plasma membrane-cell wall connections [3, 32–35]. Here, we investigate the role of one class of candidate cell swelling sensors, mechanosensitive (MS) ion channels [12, 32, 36].

MS ion channels are multimeric proteins embedded in the membrane that mediate ion flux across the membrane in response to lateral membrane tension and are found in all kingdoms of life [37–39]. Rapid cell swelling is likely to lead to an immediate increase in membrane tension, leading to the opening of MS ion channels and thereby to the exit of osmolytes and/or the entry of calcium signals that regulate downstream adaptive events. In plants, the overexpression of members of the Mid1-complementing activity (MCA) family leads to increased Ca^{2+} uptake in response to hypo-osmotic shock in *Arabidopsis*,

tobacco, and rice, but *MCA* genes are not strictly required for swelling-induced Ca^{2+} uptake [13, 18, 19]. MCA1 is also required for cell wall integrity signaling [40–42]. Members of the MscS-like (MSL) family of MS ion channels have been implicated in osmotic homeostasis in chloroplasts [43, 44] and pollen [45], but a direct function in cell swelling perception and signal transduction has not yet been demonstrated.

Arabidopsis thaliana MSL10 is an excellent candidate for a general sensor of cell swelling in plant cells. It is a MS ion channel directly gated by lateral membrane tension as indicated by single-channel patch-clamp electrophysiology [46, 47]. MSL10 is essentially non-selective with a slight preference for anions and has a conductance of about 100 pS. Expression of a *MSL10p::GUS* reporter and publicly available databases indicate that MSL10 is ubiquitously expressed at relatively low levels [46, 48–50].

Overexpression of *MSL10-GFP* leads to dwarfing, the induction of cell death, the hyperaccumulation of ROS, and upregulation of a suite of genes associated with cell death and ROS [51]. These same phenotypes are also observed in the ethyl methanesulfonate-induced gain-of-function mutant *msl10-3G*, also called *rea1* [48, 52]. The ability of MSL10 to induce all of these phenotypes is inhibited by the presence of phosphomimetic lesions at seven sites in its soluble N terminus and is promoted by the presence of phospho-dead lesions at these same sites [51, 52]. Our understanding of MSL10 function has been limited to the effects of these gain-of-function alleles, and its normal physiological role remains unclear. Here, we describe our efforts to test the hypothesis that MSL10 serves as a sensor of membrane tension during cell swelling.

RESULTS

We developed a seedling-based assay to determine the role played by MS ion channels in cell swelling responses (Figure 1A). We first assessed cell death after swelling by quantifying the uptake of the viability dye Evans blue. Seedlings were germinated and grown vertically on solid Murashige and Skoog media supplemented with either 140 mM mannitol or −0.5 MPa polyethylene glycol (PEG). Growth on these media did not affect germination rate (approximately 75%) or root growth in a genotype-specific manner (Figures S1A–S1D). After 5 to 6 days, seedlings were transferred to liquid media containing mannitol or PEG and either isoxaben (ISX) or 2,6-dichlorobenzonitrile (DCB), two inhibitors of cellulose biosynthesis [53]. Seedlings were incubated with gentle shaking for 4 h and then moved to solutions with or without mannitol or PEG for iso- or hypo-osmotic treatments, respectively. Hypo-osmotic treatment led to root cells that were significantly wider compared to iso-osmotic treatment, but increases in cell length or cell bursting rates were not observed (Figures S1E–S1H).

Cell Swelling Induces Cell Death

In wild-type seedlings, cell death increased an average of 1.6-fold after 6 h of hypo-osmotic treatment, although no significant increase was observed with iso-osmotic treatment (Figures 1B and S2A). Similar results were obtained when PEG-infused agar was used in place of mannitol (Figure 1C) or when DCB was used instead of ISX (Figure 1D). Seedlings treated with mannitol, PEG, ISX, or DCB alone did not show an increase in cell death with hypo-osmotic treatment, though seedlings grown on 330 mM mannitol alone did (Figures S2B and S2C). Although the seedlings remained submerged for the entire duration of cell swelling assay, no increase in cell death was detected after iso-osmotic treatment, indicating that anoxia did not contribute, nor did shaking during the assay (Figure S2D). Collectively, these results indicate that a combination of cell wall biosynthesis inhibition and cell swelling leads to increased cell death in *Arabidopsis* seedlings.

MSL10 Promotes Cell Swelling-Induced Cell Death

We next determined the role of MSL10 in cell swelling-induced cell death in seedlings. As shown in Figures 1B–1D, MSL10 was required for cell death in response to cell swelling in all three treatment regimens (mannitol + ISX, PEG + ISX, and mannitol + DCB). First, *msl10-1* null mutants did not show any increase in cell death after 6 h of hypo-osmotic swelling, although *msl10-1* null mutants complemented with the wild-type genomic copy of *MSL10* (*MSL10g*) had cell death levels indistinguishable from the wild type in all treatment regimes. Second, a heightened cell death response was observed in *msl10-3G* gain-of-function mutants (1.4-fold, 1.5-fold, and 1.8-fold increases over the wild type at 6 h). Quantitative gene expression analysis revealed no induction of *MSL10* transcripts in response to either iso-osmotic or hypo-osmotic treatments in any of the genotypes tested (Figure 1E), and the amounts of cell swelling and bursting in *msl10-1* and *msl10-3G* lines were indistinguishable from the wild type (Figures S1E–S1H).

We also investigated whether *PLANT DEFENSIN1.2* (*PDF1.2*) and *PEROXIDASE34* (*PERX34*), two genes previously known to be upregulated in *MSL10* gain-of-function lines [48, 51, 52], were also upregulated in response to cell swelling. In the wild type, *PDF1.2* transcript levels increased 3.8-fold and *PERX34* transcript levels increased 2.2-fold in response to cell swelling (Figure 1E). The *msl10-3G* mutant displayed an even higher expression of *PDF1.2* and *PERX34* in response to cell swelling, whereas no change in the expression of either of these two genes was observed in *msl10-1* null mutant seedlings. Thus, an MSL10-dependent mechanism leads to increased cell death in response to cell swelling and is likely related to the phenotypes observed in *MSL10* gain-of-function lines.

MSL10 Potentiates a Transient Increase in Cytoplasmic Calcium in Response to Cell Swelling

We next used the calcium-activated luminescence of Aequorin [54, 55] to determine whether $[Ca^{2+}]_{cyt}$ increases in response to cell swelling and to evaluate any role for MSL10. Wild-type, *msl10-1*, and *msl10-3G* seedlings expressing Aequorin were challenged with hypo-osmotic or iso-osmotic treatments using the injection function of a plate reader. In wild-type seedlings, $[Ca^{2+}]_{cyt}$ rose sharply within 2 s of hypo-osmotic treatment (black arrow) and then rapidly declined to a level close to baseline (Figures 2A and 2B). In *msl10-1* null mutants, this peak was diminished, and *msl10-3G* seedlings showed a much higher peak of $[Ca^{2+}]_{cyt}$ in response to cell swelling than wild-type seedlings. Quantitation showed that the $[Ca^{2+}]_{cyt}$ response to hypo-osmotic treatment in the *msl10-1* mutant was significantly lower than in

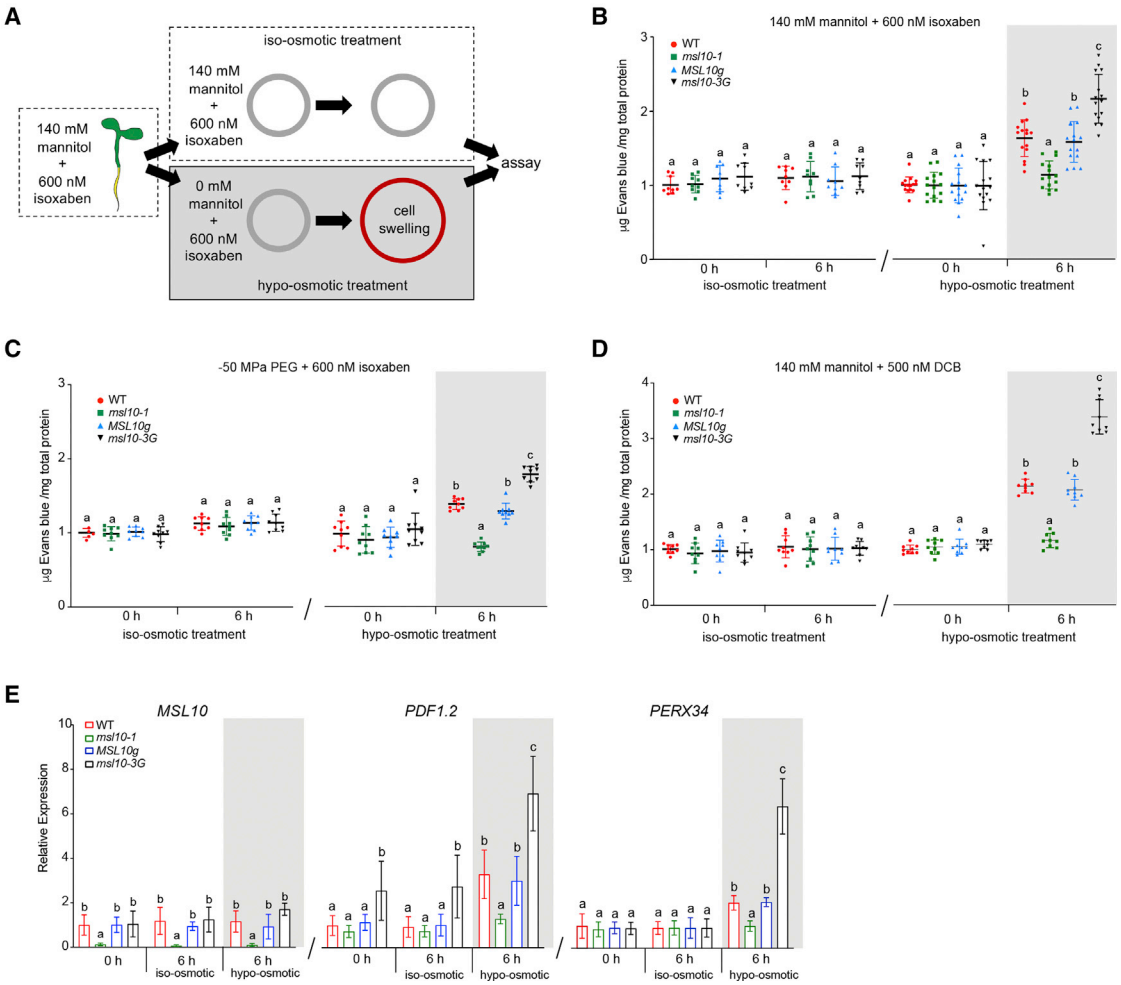

Figure 1. Cell Swelling Results in MSL10-Dependent Cell Death

(A) The seedling cell swelling assay and expected effects of each treatment on a single cell.

(B–D) Evans blue uptake normalized to iso-osmotic treatment of the wild type at 0 h. 5-day-old seedlings were incubated in culture media supplemented with 140 mM mannitol (B and D) or with −0.5 MPa PEG (C) and either 600 nM ISX (B and C) or 500 nM DCB (D) for 4 h and then subjected to either iso-osmotic or hypo-osmotic treatments. Results from five (B) or three (C and D) independent trials are shown. Each trial included three replicates of a pool of six seedlings for each genotype/treatment combination.

(E) Quantitative RT-PCR analysis showing transcript levels relative to the wild type in seedlings treated as in (B). Results from three independent trials are shown. Each trial included three technical replicates of a pool of 18 seedlings for each genotype/treatment combination. Error bars represent standard deviation between the means.

For all panels, two-way ANOVA with Tukey's post hoc test was used to assess statistical differences; different letters denote significant differences ($p < 0.05$). See also Figures S1 and S2.

the wild type at both 5.6 and at 7.8 s after the start of the experiment and closely resembled the wild-type response to iso-osmotic treatment (Figures 2C and 2D). The $[Ca^{2+}]_{cyt}$ response in the *msl10-3G* mutant was significantly higher than the wild type at 5.6 s. Thus, cell swelling triggers a rapid and transient increase in $[Ca^{2+}]_{cyt}$ and MSL10 is required for this response. Although most previous reports of $[Ca^{2+}]_{cyt}$ response to hypo-osmotic shock describe a biphasic response [11, 15, 20, 21], these responses vary widely in timescale and relative peak heights, and in some cases, a monophasic response is observed [14, 18, 25]. These differences can be attributed to differences in the tissue used, the extent of osmotic down shock, and the timescale of measurement.

MSL10 Potentiates ROS Accumulation in Response to Cell Swelling

As ROS accumulation is commonly associated with the induction of various types of programmed cell death (PCD) in plants [56, 57] and plants harboring *MSL10* gain-of-function alleles display increased ROS accumulation [51, 52], we wished to determine whether cell swelling triggers ROS accumulation and to investigate the possible role of MSL10 in that process. 5-day-old seedlings subjected to cell swelling were stained with the ROS indicator dye 2, 7-dichlorofluorescein diacetate (H_2DCFDA), and fluorescence intensities were measured using a laser scanning confocal microscope (Figure S4A). By 30 min, cell swelling produced a 2-fold increase in H_2DCFDA

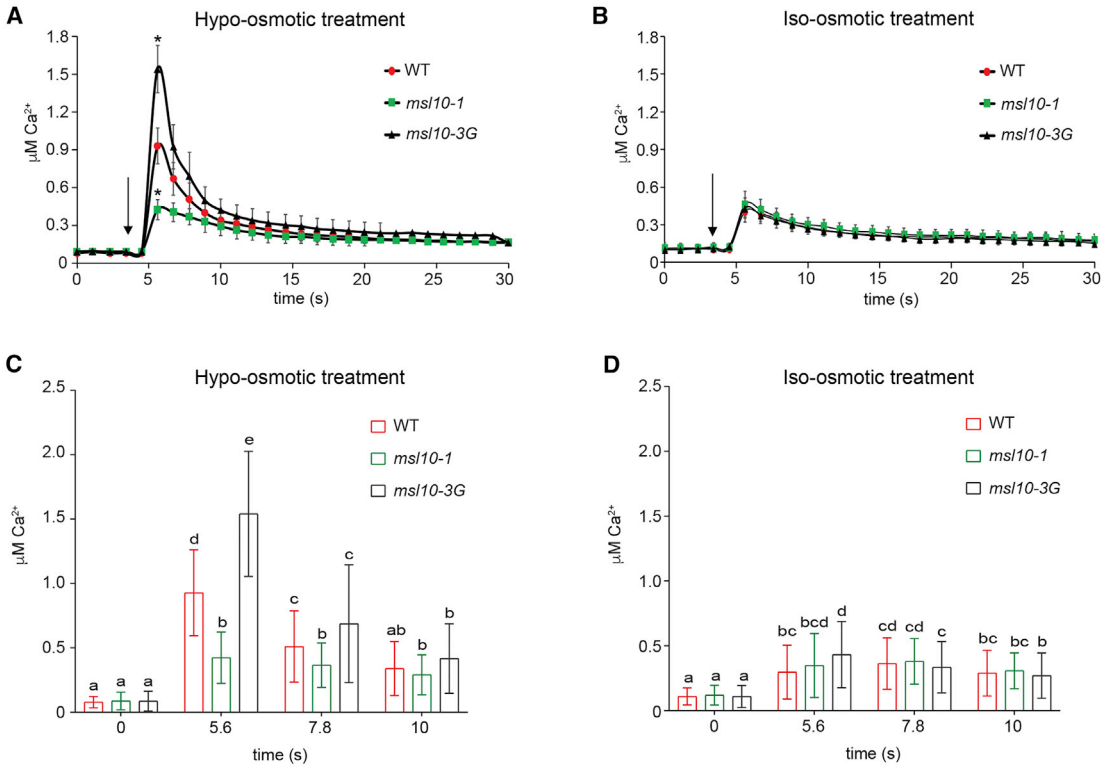

Figure 2. MSL10 Potentiates a Transient Increase in Cytoplasmic Calcium in Response to Cell Swelling

(A and B) Time courses of $[Ca^{2+}]_{cyt}$ in 3- to 4-day-old Aequorin-expressing seedlings incubated in ISX for 4 h and then diluted with deionized water (A) or 140 mM mannitol (B) to produce hypo- or iso-osmotic treatments by auto-injection in a plate reader (arrows). Errors bars indicate standard error of the means from four independent trials, each including three transgenic lines per genotype, 7 seedlings per line. Variation among individual transgenic lines is shown in Figure S3. (C and D) $[Ca^{2+}]_{cyt}$ levels from the data shown in (A) and (B), respectively, before treatment (2.2 s after the start of the experiment), at the apex of the main peak (5.6 s after the start of the experiment), and at two points during recovery (7.8 and 10 s after the start of the experiment). Error bars and statistical analyses are as in Figure 1.

fluorescence intensity in wild-type seedlings (Figure 3A). At this same time point, no increase in ROS was observed in *msl10-1* null mutants, accumulation was recovered in the *MSL10g* lines, and *msl10-3G* lines accumulated high levels of ROS (almost a 4-fold increase over the iso-osmotic treatment). Iso-osmotic treatment did not induce ROS accumulation beyond a small increase in *msl10-3G* lines.

We next attempted to localize the source of cell swelling-induced ROS by including inhibitors in the cell swelling treatment solutions. We tested diphenyleneiodonium (DPI) (generally considered to be an NADPH oxidase inhibitor; but see [58]), potassium iodide (KI) (a scavenger of H_2O_2), or salicylhydroxamic acid (SHAM) (a peroxidase inhibitor) [18, 23, 59]. DPI had the strongest effect, reducing ROS levels in the wild-type and *MSL10g* lines to that of untreated controls and also reducing levels in *msl10-3G* lines (Figure 3B). Including KI and SHAM in cell swelling treatments had only modest effects on H_2DCFDA fluorescence intensity. Thus, most, but not all, of the ROS produced in response to cell swelling is dependent on MSL10 and likely involves the action of NADPH oxidases.

To further confirm the role of MSL10 in early ROS accumulation after cell swelling, we used the ROS-dependent fluorescence of cytoplasmic roGFP1, a ratiometric fluorescent biosensor that is used to report intracellular levels of ROS [60]. roGFP1 signal increased in wild-type seedlings after 30 min of hypo-osmotic treatment (Figure 3C), although *msl10-1* seedlings did not show any increase in roGFP1 signal. In *msl10-3G* mutants, roGFP1 signal was significantly higher than the wild type at both 30 and 60 min after hypo-osmotic treatment. For calibration, seedlings were treated with either 10 mM H_2O_2 or 10 mM dithiothreitol (DTT) to fully oxidize or reduce roGFP1 (Figure S4B). Thus, cell swelling leads to increased ROS levels within 30 min after treatment and MSL10 is required for the early stage of this response.

MSL10 Potentiates Hypo-osmotic Shock-Associated Changes in Gene Expression

It was previously observed that several genes implicated in touch and mechano-response are induced in *Arabidopsis* root tips after 20 min of hypo-osmotic treatment [21]. In wild-type seedlings, transcript levels of *TCH1*, *TCH2*, *TCH3*, and *TCH4* increased by 6- to 22-fold after 30 min of cell swelling; level began to decrease after 60 min (Figure 4). *WRKY18* transcripts also increased after cell swelling but with different temporal dynamics, showing a 4-fold increase in transcript levels after 30 min and a 12-fold increase after 60 min of hypo-osmotic treatment. *MSL10* was required for full induction of all of these genes in response to hypo-osmotic swelling, as *msl10-1*-null mutants

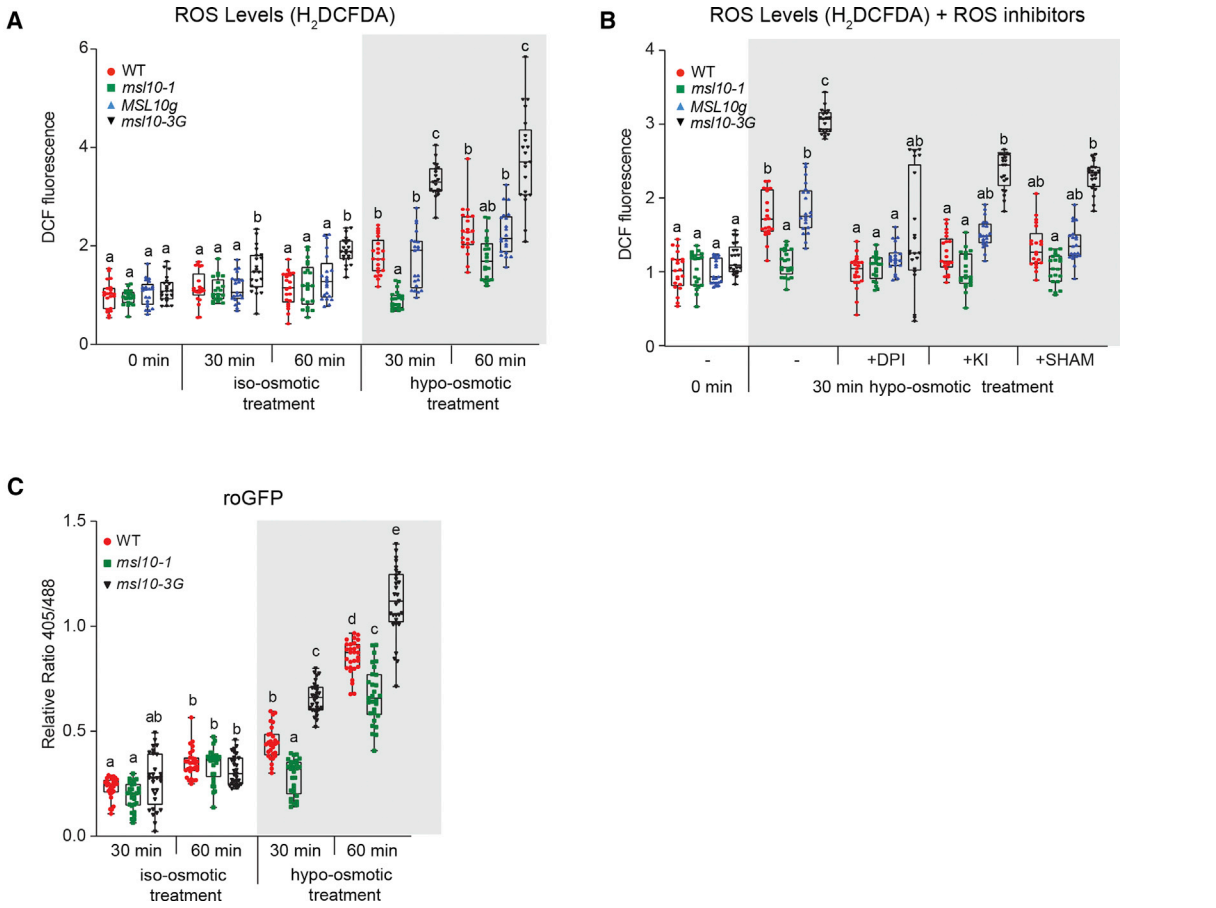

Figure 3. MSL10 Potentiates ROS Accumulation in Response to Cell Swelling

(A) Quantification of H_2DCFDA fluorescence in 5-day-old seedlings in response to cell swelling. Results from three independent trials are shown. Each trial included 5–10 seedlings for each genotype/treatment combination.

(B) Effect of inhibitors on ROS accumulation during cell swelling as detected by H_2DCFDA staining. Results from three independent trials are shown. Each trial included seven seedlings for each genotype/treatment combination.

(C) Relative change in roGFP1 oxidation upon cell swelling as calculated from the measured intensity ratios (405/488 nm). 5-day-old seedlings were subjected to cell swelling, and fluorescent intensity ratios were quantified from confocal images of root transition/elongation zones. Results from three independent trials are shown. Each trial included 9 to 10 seedlings for each genotype/treatment combination.

For all panels, error bars and statistical analyses are as in Figure 1. See also Figure S4.

exhibited about half the transcript increases observed in wild-type seedlings. Transcripts from all five genes in *MSL10g* lines were indistinguishable from the wild type, and the gain-of-function line *msl10-G* showed an even higher increase in transcript levels. Taken together, the results presented in Figures 2, 3, and 4 show that cell swelling activates a number of downstream responses previously associated with hypo-osmotic shock, including a burst of $[Ca^{2+}]_{cyt}$, a burst of ROS, and the transient induction of mechano-inducible genes.

Cell Swelling Results in MSL10-Dependent Programmed Cell Death

PCD is a generic term used for multiple processes that result in cellular suicide in both plants and animals [61] and in plants can be generally categorized as developmentally induced (dPCD), pathogen-induced (pPCD), or environmentally induced (ePCD) [62–64]. As identifying and categorizing PCD-like events in plants has proven difficult and controversial [61, 65], we used a set of well-established assays for PCD to test whether cell swelling-induced cell death could be classified as PCD.

First, we used the terminal deoxynucleotidyl transferase dUTP nick end labeling (TUNEL) assay [66] to measure DNA fragmentation in root cells of seedlings subjected to cell swelling. Six hours after cell swelling, the number of TUNEL-positive nuclei doubled in wild-type seedlings (Figures 5A and S5A). Furthermore, this increase required MSL10, as no increase over iso-osmotic treatment was observed in *msl10-1* mutants, and levels were restored in the complemented *MSL10g* line. The *msl10-3G* gain-of-function line showed even higher levels of cell swelling-induced TUNEL staining (a 5-fold increase after 6 h of cell swelling). As expected, essentially all cells had TUNEL-positive nuclei when wild-type seedlings were incubated with DNase I for 15 min prior to the TUNEL reaction, and no TUNEL-positive nuclei were detected when the terminal deoxynucleotidyl transferase enzyme was omitted from the TUNEL reaction mixture (Figures S5B and S5C).

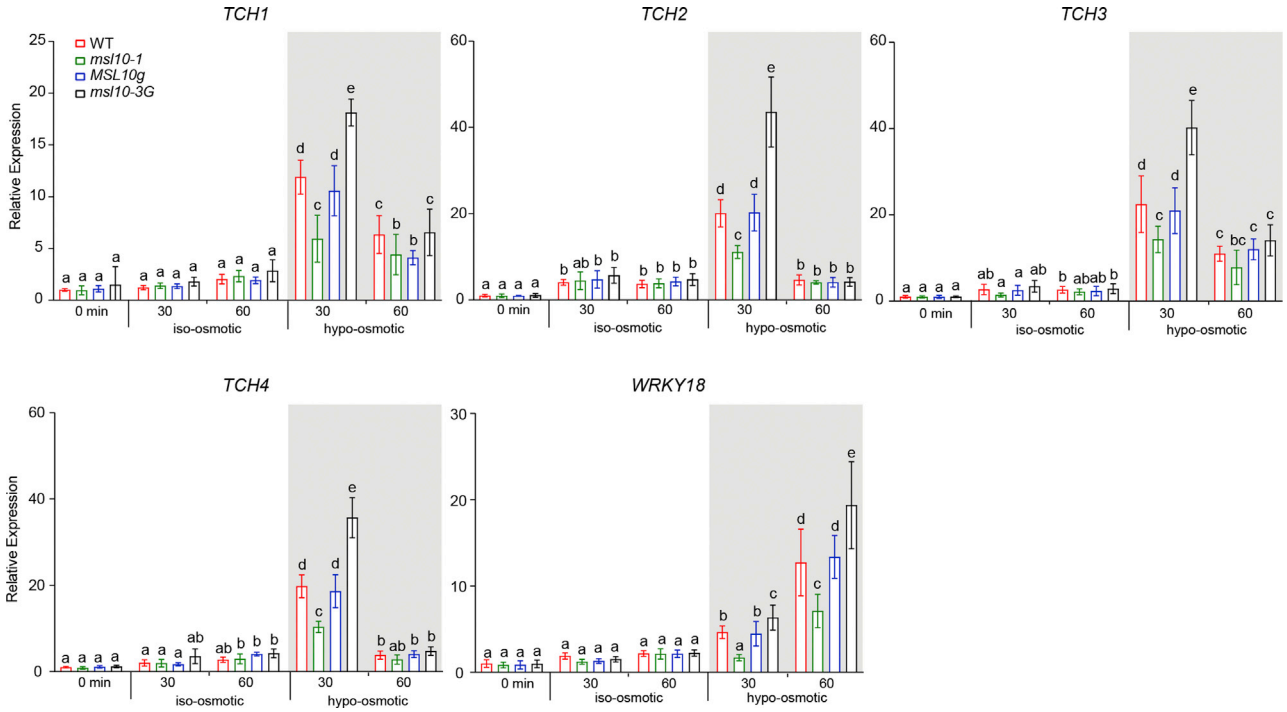

Figure 4. MSL10 Potentiates Hypo-osmotic Treatment-Associated Gene Expression

Quantitative RT-PCR analysis of genes implicated in hypo-osmotic stress response in seedlings after cell swelling, performed and analyzed as in Figure 1E.

Next, we used a commercial fluorometric caspase-3 activity assay to assess the activation of cysteine proteinases (caspase-like proteases) [67] in protein extracts from whole seedlings as in [68, 69]. Wild-type and complemented *MSL10 g* seedlings displayed increased caspase-3-like protease activity after cell swelling (from 5 to 140 and 134 units/μg of total protein after 3 h, respectively; Figure 5B). We observed a significantly reduced induction of caspase-3-like activity in *msl10-1* mutant seedlings and a significantly larger induction in *msl10-3G* mutant seedlings, in response to cell swelling compared to the wild type. Extracts from 1-h, 3-h, and 6-h samples that were treated with the caspase-3 inhibitor Ac-DEVD-CHO were indistinguishable from the 0-h time point, indicating that the activity detected is specific to the caspase-3-like protease family.

Cytoplasmic acidification is another cellular marker of plant PCD [70], and an increase in vacuolar pH can be used as a proxy for cytoplasmic acidification [71, 72]. We stained seedlings with the vacuolar pH indicator dye 2,7-bis-(2-carboxyethyl)-5-(and-6)-carboxy-fluorescein acetoxy-methyl ester (BCECF-AM) [73] (Figures S5D and S5E). After 3 h of cell swelling, we observed an increase in the vacuolar pH of wild-type seedling root cells (Figure 5C). *msl10-3G* mutant seedlings displayed a greater increase in vacuolar pH in response to cell swelling than wild-type seedlings, whereas no significant increase in vacuolar pH was observed in *msl10-1* mutant seedlings.

We next turned to marker gene expression to understand what type of PCD is induced by cell swelling. *BIFUNCTIONAL NUCLEASE I* (*BFN1*), *RIBONUCLEASE 3* (*RNS3*), and *METACASPASE 9* (*MC9*) are three of the nine genes belonging to the core "developmental cluster" known to be induced during dPCD, but not during ePCD [62]. *MC9* may also be involved in biotic stress [74]. *BFN1* and *RNS3* expression levels did not change significantly in response to iso-osmotic treatment or to cell swelling in any of the genotypes at any time points tested (Figure 5D). *MC9* levels also did not change, except for a small increase in *msl10-3G* seedlings after 3 h of cell swelling (Figure 5E). These data indicate that cell swelling-induced PCD is distinct from known dPCD.

Finally, we measured transcript levels of *METACASPASE 1* (*MC1*) and *METACASPASE 2* (*MC2*) in response to cell swelling. *MC1* and *MC2* are metacaspase genes implicated in PCD and are associated with both biotic and abiotic stress responses [74–77]. In wild-type seedlings, *MC1* and *MC2* transcript levels increased 4- to 6-fold after 1 h and 3 h of cell swelling, respectively (Figure 5E). In contrast, *msl10-1* null mutants only displayed a slight increase in expression of *MC2*, whereas *msl10-3G* mutants displayed a marked increase in *MC1* and *MC2* expression (10-fold and 10.5-fold, respectively). Taken together, the data presented in Figure 5 show that cell swelling induces PCD that is distinct from dPCD and that these effects either require or are promoted by the mechanosensitive ion channel MSL10.

Cell Swelling-Induced PCD Is Prevented by Phosphomimetic Amino Acid Substitutions in the MSL10 N Terminus

We previously showed that overexpressed MSL10-GFP is unable to trigger cell death when four residues in its soluble N-terminal domain are replaced with phosphomimetic residues (MSL10 S57D, S128D, S131E, and T136D, denoted MSL10^{4D}-GFP) [51]. Conversely, replacing these four residues along with three others in the N terminus with alanine (MSL10^{7A}-GFP) produces constitutive cell death in a transient expression system [51]. We therefore

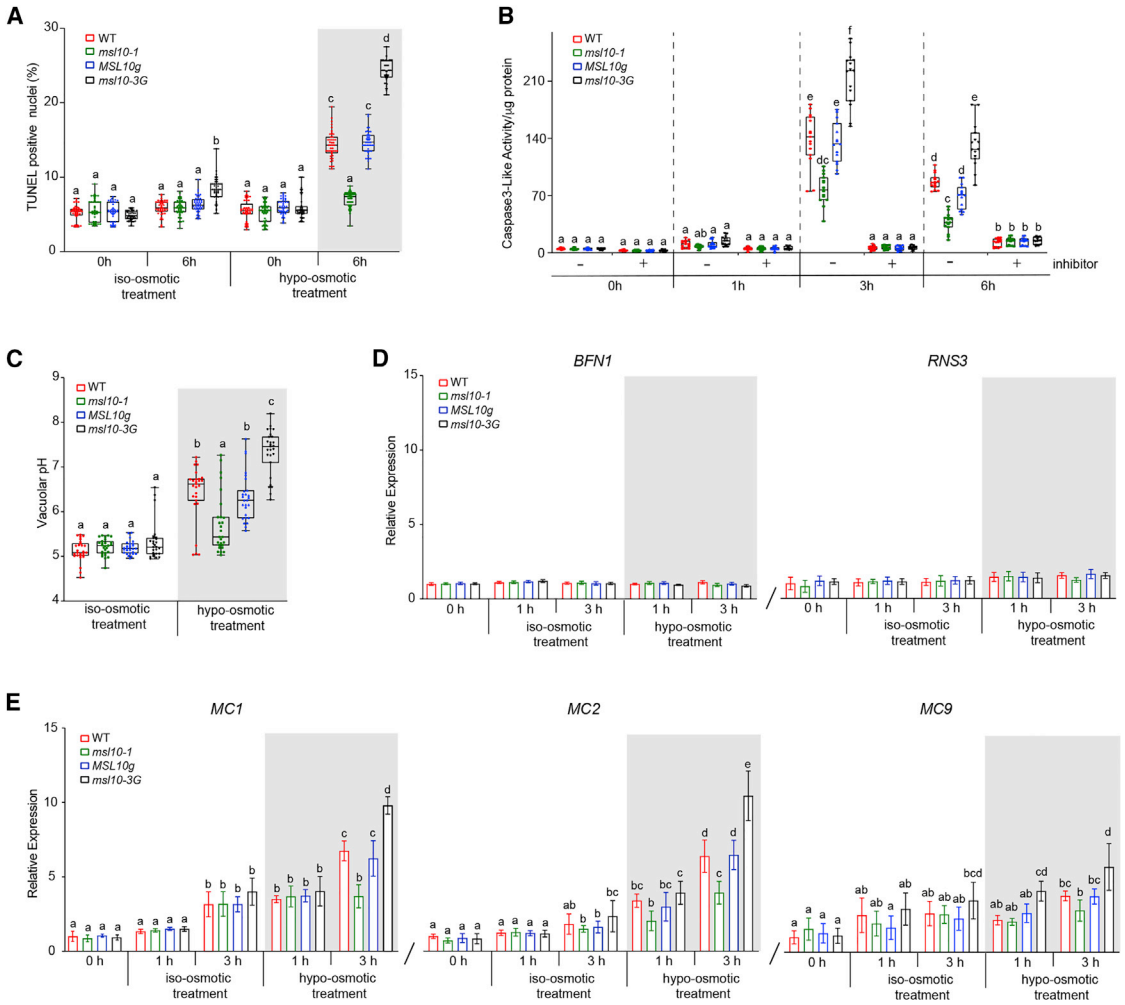

Figure 5. Cell Swelling Results in MSL10-Dependent Programmed Cell Death

(A) Frequency of TUNEL-positive nuclei in the root tip of seedlings after iso-osmotic or hypo-osmotic treatment. Results from three independent trials of 15 seedlings from each genotype/treatment combination are presented.

(B) Caspase-3-like activity in response to cell swelling. Homogenates isolated from 7-day-old seedlings that underwent cell swelling were incubated with 50 µM Ac-DEVD-AMC for 1 h. Some extracts were treated with 100 µM Ac-DEVD-CHO for 1 h before the assay. Results from three independent trials are shown. Each trial included five replicates of a pool of six seedlings for each genotype/treatment combination.

(C) Increase in vacuolar pH in response to cell swelling as indicated by the pH-sensitive fluorescent dye BCECF-AM. Results from three independent trials of 9 seedlings from each genotype/treatment combination are presented.

(D and E) Quantitative RT-PCR analysis of dPCD-responsive genes (D) and ePCD-responsive genes (E) in response to cell swelling, performed as for Figure 1E. For all panels, error bars and statistical analyses as in Figure 1. See also Figure S5.

decided to examine the effect of these same N-terminal substitutions on cell swelling-induced PCD.

Lines overexpressing *MSL10-GFP* from the strong, constitutive 35S promoter showed significantly more swelling-induced cell death than the wild type (3.5-fold versus 1.7-fold increase in Evans blue uptake and 21% versus 11% TUNEL-positive nuclei, respectively; Figures 6A and 6C). Lines constitutively overexpressing *MSL10^{4D}-GFP* at high levels did not induce PCD in response to cell swelling and were indistinguishable from the *msl10-1* mutant. Immunoblotting indicated that MSL10-GFP and MSL10^{4D}-GFP accumulated to similar levels in these lines (Figure 6B). It is not possible to isolate lines stably expressing phospho-dead versions of MSL10-GFP from the 35S promoter [51].

Expressing untagged *MSL10* from its endogenous promoter in the *msl10-1* mutant background produced cell swelling-induced PCD at levels comparable to the wild type (Figure 6D), and conditional overexpression of untagged *MSL10* from a dexamethasone-inducible promoter produced even more PCD in response to cell swelling than the wild type (Figure 6E). Endogenous expression of *MSL10g^{7A}* (but not *MSL10g^{7D}*) or conditional expression of phospho-dead *DEX::MSL10^{4A}* (but not *DEX::MSL10^{4D}*) resulted in more cell swelling-induced PCD than wild-type seedlings. We were unable to assess MSL10 protein levels in these lines, but transcripts from *MSL10g* transgenes were similar to endogenous levels, and transcripts from *DEX::MSL10* transgenes were induced in the presence of dexamethasone (Figure S6).

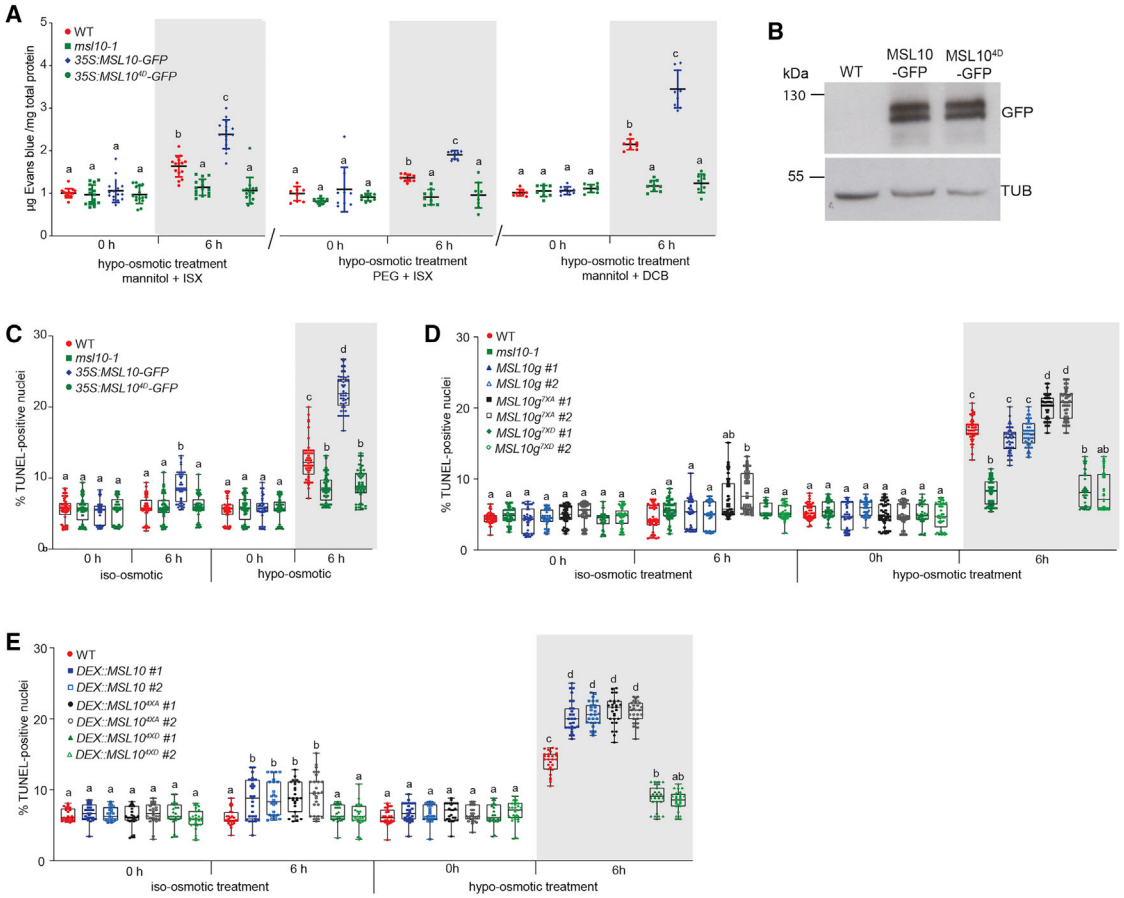

Figure 6. Cell Swelling-Induced PCD Is Prevented by Phosphomimetic Amino Acid Substitutions in the MSL10 N Terminus

(A) Swelling-induced cell death in lines overexpressing *MSL10-GFP* and *MSL10^{4D}-GFP*, as measured by Evans blue uptake as described for Figure 1. Results from five independent trials are shown. Each trial included three replicates of a pool of six seedlings for each genotype/treatment combination.

(B) Immunodetection of MSL10-GFP variant proteins. Total protein was isolated from 6 pooled 5-day-old seedlings grown on media supplemented with 140 mM mannitol. An anti-GFP primary antibody was used to detect MSL10-GFP (top panel) and the blot re-probed with an anti-α-tubulin primary antibody (bottom panel). Theoretical molecular masses of proteins are indicated at the left according to a commercially available standard. Presence of two bands may be attributed to posttranslational modification.

(C) *In situ* detection of DNA fragmentation in lines overexpressing MSL10-GFP and MSL10^{4D}-GFP using the Click-iT TUNEL Alexa Fluor 647 Imaging Assay kit. Results from three independent trials are shown. Each trial included 15 seedlings from each genotype and treatment.

(D) Detection of *in situ* DNA fragmentation in response to cell swelling in seedlings expressing *MSL10g*, *MSL10g^{7A}*, or *MSL10g^{7D}* in the *msl10-1* background, as described for Figure 5A. Results from three independent trials are shown. Each trial included 10–20 seedlings from each genotype and treatment.

(E) Detection of *in situ* DNA fragmentation in response to cell swelling wild-type seedlings expressing *DEX:MSL10*, *DEX:MSL10^{4A}*, and *DEX:MSL10^{4D}*, as described for Figure 5A. Seedlings were incubated with 30 µM DEX in media supplemented with 140 mM mannitol during the equilibration step. Results from three independent trials are shown. Each trial included 9 seedlings from each genotype and treatment.

For (A) and (C)–(E), error bars and statistical analyses are as in Figure 1. See also Figure S6.

Thus, introducing phosphomimetic lesions into the MSL10 N terminus prevented PCD in response to cell swelling. Furthermore, the effect cannot be attributed to the presence of a GFP tag, to non-specific effects of MSL10 overexpression, or to a developmental response to the presence of high levels of MSL10. These results are consistent with the proposal that dephosphorylation of the MSL10 N terminus is required for cell swelling-induced PCD.

DISCUSSION

Here, we establish and validate a procedure for imposing cell swelling on whole *Arabidopsis* seedlings. We show that cell swelling induces programmed cell death, ROS accumulation, the transient elevation of cytoplasmic Ca^{2+}, and the expression of mechano-inducible genes. Furthermore, we show that MSL10 positively influences all these steps in the swelling-induced signaling pathway and that this effect is regulated by phosphorylation of the soluble MSL10 N terminus.

Cell Swelling in Response to Cell Wall Softening and Hypo-osmotic Treatment

Plant cell mechanics are primarily determined by the dynamic interplay between the cell wall and turgor pressure. The plant cell wall is a complex arrangement of cellulose microfibrils, hemicelluloses, pectins, and glycoproteins that has incredible tensile

strength yet can be finely tuned in order to generate cell shape, allow growth, and protect cell integrity [78]. Although the directionality of any changes in cell volume is controlled by the orientation of cellulose microfibrils and the local stiffness of pectin, the driving force is turgor pressure, the pressure that the protoplast exerts on the cell wall (up to multiple atmospheres) [79]. Importantly, the plasma membrane (and therefore any embedded mechanosensitive ion channels) sits at the interface between cell wall strength and turgor pressure. Under normal conditions, turgor pressure and cell wall strength are in balance, but when the cell wall softens or turgor increases, cell swelling occurs and membrane tension increases.

In this study, we used a combination of cell wall softening (accomplished by treatment with the cellulose synthase inhibitor ISX) and increased turgor (accomplished by transferring plants to a hypo-osmotic solution) to activate downstream cell swelling signaling pathways and provide a tool for dissection of the process (Figure 1A). Although we did not observe any increased cell death after 6 h of treatment with ISX or DCB alone in our assay (Figure S2B), inhibition of cell wall biosynthesis has been reported to induce cell death after 10–24 h of treatment [40, 80–83]. In addition, ISX or DCB treatment alone can induce apoplastic ROS accumulation and lead to increased *PDF1.2* and *TCH4* transcript levels [41, 83–85]. Furthermore, our results can be recapitulated without cell wall softening if a larger osmotic down shock is used, presumably because it produces the same level of cell swelling (Figure S2C). Thus, inhibition of cell wall synthesis, hypo-osmotic shock, or a combination of the two all lead to similar downstream signaling events.

MSL10 as a Cell Swelling Sensor

The data presented here support a model wherein MSL10 is the primary plasma-membrane-based sensor of cell swelling in Arabidopsis seedlings. MSL10 positively influences all previously documented downstream effects of hypo-osmotic shock that we tested. Cell death (Figure 1), a burst of $[Ca^{2+}]_{cyt}$ (Figure 2), accumulation of ROS (Figure 3), and increased transcript levels for four mechano-inducible genes (Figure 4) were reduced or absent in the *msl10-1* null mutant and enhanced in the *msl10-3G* gain-of-function line. In addition, four distinct hallmarks of programmed cell death—DNA fragmentation, increased caspase-like activity, cytosolic acidification, and PCD-associated gene expression—increased in response to cell death in a MSL10-dependent manner. Particularly suggestive is the observation that the transient increase in $[Ca^{2+}]_{cyt}$ levels observed in *msl10-1* plants in response to hypo-osmotic treatment is indistinguishable from the response to iso-osmotic treatment. The latter is likely to be a mechanical response to injection of the treatment solution. These data indicate that the perceptive events that occur within the first 2 s of swelling require MSL10. The immediacy of this effect and its complete requirement for MSL10 provide strong evidence that MSL10 directly receives a swelling signal at the membrane to potentiate downstream effects.

Notably, this is the first reported loss-of-function phenotype for *MSL10* other than a modest, and presumably indirect, defect in starch degradation [86]. Despite a decade of research, plants lacking functional MSL10 have performed identically to the wild type in numerous developmental and mechanical stress assays [21, 46, 87–90]. Until now, genetic evidence for MSL10 function has been derived solely from the phenotypes associated with MSL10 gain-of-function alleles: the overexpression of *MSL10-GFP*; the expression of untagged $MSL10g^{7A}$ from the endogenous promoter; or the *msl10-3G* allele [48, 51, 52]. In these backgrounds, phenotypic effects, such as dwarfing and ectopic cell death, are apparent in adult plants without added stress, though seedlings are indistinguishable from the wild type. In the experiments presented here, these gain-of-function lines required cell swelling to produce substantial increases in cell death, PCD, $[Ca^{2+}]_{cyt}$ transients, ROS accumulation, or gene expression. *MSL10-GFP*, *msl10-3G*, and $MSL10g^{7A}$ lines did eventually have a stronger response than the wild type, and we speculate that the consistent environment of defined media and a younger age resulted in a lower baseline of MSL10 activity than when these same lines are grown for longer periods of time and on soil. Signaling in response to cell swelling is therefore likely to be the normal function of the MSL10 protein and not the result of toxic or non-physiological effects.

We previously used single-channel patch-clamp electrophysiology to demonstrate that the MSL10 channel opens in response to increased lateral membrane tension and that this does not require association with other cellular components [47]. Thus, one straightforward interpretation of the data presented here is that cell swelling increases membrane tension, which opens the MSL10 channel and provides an ionic signal that activates the rest of the downstream pathway. However, MSL10 has a preference for anions, and electrophysiological experiments with large ions suggest that it does not conduct Ca^{2+} [46, 47, 91]. As MSL10 has a relatively long closing time [47], one possibility is that an extended release of Cl^- ions through the MSL10 channel pore leads to depolarization of the plasma membrane and the subsequent activation of depolarization-activated Ca^{2+} channels [92].

Another possibility is that MSL10's ability to induce cell death, PCD, $[Ca^{2+}]_{cyt}$ transients, ROS accumulation, and gene expression is independent of its ion channel function. Several lines of evidence suggest that MSL10 has a non-conducting function that is mediated through its soluble N-terminal domain: (1) phosphomimetic lesions in the soluble N terminus prevent *MSL10* from inducing ROS accumulation and cell death, and phospho-dead lesions exacerbate these effects [51, 52]; (2) neither type of lesion affects MSL10's mechanosensitive ion channel activity when expressed in oocytes [51]; and (3) MSL10 variants with pore-blocking mutations are able to induce cell death when transiently overexpressed in tobacco cells [93]. As expression of phosphomimetic variants of MSL10 also prevented cell swelling-induced PCD (Figure 6), this function may be independent of ion flux through the MSL10 channel pore. Future work to determine whether pore-blocking mutations influence MSL10-dependent responses to cell swelling may help answer this question.

We have proposed that tension-induced conformational changes in MSL10 lead to dephosphorylation of the N terminus through a three-step mechanism [52]. We speculate here that dephosphorylation of the MSL10 N terminus promotes its interaction with a Ca^{2+} channel, thereby potentiating a burst of $[Ca^{2+}]_{cyt}$ and the other downstream events that eventually lead to PCD. Either through this mechanism or through the effects on ion flux or membrane potential

mentioned above, the combined action of MSL10 and a calcium channel could together provide the elusive stretch-activated Ca^{2+} channel activity long proposed to mediate cell swelling responses [12, 32, 36].

The data shown in Figure 5 show that cell swelling induces a type of PCD that is distinct from developmentally regulated PCD and may be similar to that induced by biotic or other abiotic stresses, such as heat, salt stress, flooding, or dehydration [64, 94]. The induction and execution of PCD in plants, as in animals, involves a huge number of molecular signals and communication between multiple subcellular compartments and organelles [61]. As a result, we employed four distinct assays to demonstrate that swelling-induced cell death can be classified as PCD (Figure 5). These different assays produced qualitatively similar but quantitatively different results with respect to a requirement for MSL10. Cell swelling-induced increases in TUNEL-positive nuclei and cytoplasmic acidification were fully MSL10 dependent, although increased caspase-3-like protease activity and the increased expression of metacaspase genes *MC1* and *MC2* were positively influenced by, but not fully dependent on, MSL10. These differences may reflect tissue-specific differences in swelling-induced PCD, as the TUNEL assay and cytoplasmic acidification assays were performed on cells of the elongation zone of roots, and the caspase-3 activity and gene expression assays were performed on whole seedlings. Based on these results, we categorize MSL10-dependent cell swelling-induced PCD as a type of ePCD.

What, If Any, Is the Adaptive Advantage of Responding to Cell Swelling by Inducing PCD?

In the case of plant defense response, cell suicide local to the infection is thought to prevent the growth and thereby the spread of a biotrophic pathogen [95]. Abiotic-stress-induced PCD in roots is thought to promote the development of lateral roots better acclimated to salinity [96] and to produce root architectures that are more drought or flooding tolerant [97, 98]. We speculate that plants with cells likely to have experienced membrane damage due to extreme cell swelling trigger PCD, stoping growth in damaged tissues, removing damaged cells, and allowing the plant to recover materials [99].

The results presented here provide a physiological context for MSL10 function, link disparate observations regarding hypo-osmotic shock response in plant cells, and build a foundation for molecular exploration of the signaling pathway. We anticipate that future work will reveal how MSL10 functions as a membrane-based sensor that connects the perception of cell swelling to the downstream signaling cascade of abiotic-stress-induced PCD and the real-world context for its actions.

STAR★METHODS

Detailed methods are provided in the online version of this paper and include the following:

- KEY RESOURCES TABLE
- RESOURCE AVAILABILITY
  - Lead Contact
  - Materials Availability Statement
  - Data and Code Availability
- EXPERIMENTAL MODEL AND SUBJECT DETAILS
  - Plant materials
  - Accession numbers
- METHOD DETAILS
  - Generation of transgenic plants
  - Dose-dependent sensitivity of mannitol and PEG on seed germination
  - Relative root elongation
  - Cell swelling treatments
  - Evans blue quantification
  - TUNEL assay
  - Caspase-3-like activity
  - Vacuolar pH
  - Monitoring ROS
  - Measuring redox status using roGFP biosensors
  - Aequorin-based $[Ca^{2+}]_{cyt}$ luminescence
  - Gene expression analysis
  - Immunoblot analysis
- QUANTIFICATION AND STATISTICAL ANALYSIS

SUPPLEMENTAL INFORMATION

Supplemental Information can be found online at https://doi.org/10.1016/j.cub.2020.05.015.

ACKNOWLEDGMENTS

We thank the Arabidopsis Biological Resource Center for pBINU-CYA. This work was supported by the NSF Science and Technology Center Grant 1548571, NASA NNX13AM55G to E.S.H., and NSF MCB 1253103 to E.S.H.

AUTHOR CONTRIBUTIONS

D.B. and E.S.H. conceived the project and designed the experiments, D.B. performed the experiments, E.S.H. created the main-text figures, and D.B. and E.S.H. wrote the manuscript.

DECLARATION OF INTERESTS

The authors declare no competing interests.

Received: April 1, 2020
Revised: May 1, 2020
Accepted: May 5, 2020
Published: June 11, 2020

REFERENCES

1. Toft-Bertelsen, T.L., Larsen, B.R., and MacAulay, N. (2018). Sensing and regulation of cell volume - we know so much and yet understand so little: TRPV4 as a sensor of volume changes but possibly without a volume-regulatory role? Channels (Austin) *12*, 100–108.
2. Wood, J.M. (2011). Bacterial osmoregulation: a paradigm for the study of cellular homeostasis. Annu. Rev. Microbiol. *65*, 215–238.
3. Hýskova, V., and Ryslava, H. (2018). Hyperosmotic versus hypoosmotic stress in plants. Biochem. Anal. Biochem. *7*, 1–4.
4. Scharwies, J.D., and Dinneny, J.R. (2019). Water transport, perception, and response in plants. J. Plant Res. *132*, 311–324.
5. Zonia, L., and Munnik, T. (2007). Life under pressure: hydrostatic pressure in cell growth and function. Trends Plant Sci. *12*, 90–97.
6. Jayaraman, D., Gilroy, S., and Ané, J.-M. (2014). Staying in touch: mechanical signals in plant-microbe interactions. Curr. Opin. Plant Biol. *20*, 104–109.

7. Jackson, M.B., Ishizawa, K., and Ito, O. (2009). Evolution and mechanisms of plant tolerance to flooding stress. Ann. Bot. *103*, 137–142.
8. Beattie, G.A. (2011). Water relations in the interaction of foliar bacterial pathogens with plants. Annu. Rev. Phytopathol. *49*, 533–555.
9. Sugimoto, K., Himmelspach, R., Williamson, R.E., and Wasteneys, G.O. (2003). Mutation or drug-dependent microtubule disruption causes radial swelling without altering parallel cellulose microfibril deposition in Arabidopsis root cells. Plant Cell *15*, 1414–1429.
10. Droillard, M.-J., Boudsocq, M., Barbier-Brygoo, H., and Laurière, C. (2004). Involvement of MPK4 in osmotic stress response pathways in cell suspensions and plantlets of *Arabidopsis thaliana*: activation by hypoosmolarity and negative role in hyperosmolarity tolerance. FEBS Lett. *574*, 42–48.
11. Takahashi, K., Isobe, M., Knight, M.R., Trewavas, A.J., and Muto, S. (1997). Hypoosmotic shock induces increases in cytosolic Ca^{2+} in tobacco suspension-culture cells. Plant Physiol. *113*, 587–594.
12. Cazalé, A.C., Rouet-Mayer, M.A., Barbier-Brygoo, H., Mathieu, Y., and Laurière, C. (1998). Oxidative burst and hypoosmotic stress in tobacco cell suspensions. Plant Physiol. *116*, 659–669.
13. Nakagawa, Y., Katagiri, T., Shinozaki, K., Qi, Z., Tatsumi, H., Furuichi, T., Kishigami, A., Sokabe, M., Kojima, I., Sato, S., et al. (2007). Arabidopsis plasma membrane protein crucial for Ca^{2+} influx and touch sensing in roots. Proc. Natl. Acad. Sci. USA *104*, 3639–3644.
14. Nguyen, H.T.H., Bouteau, F., Mazars, C., Kuse, M., and Kawano, T. (2018). The involvement of calmodulin and protein kinases in the upstream of cytosolic and nucleic calcium signaling induced by hypoosmotic shock in tobacco cells. Plant Signal. Behav. *13*, e1494467.
15. Pauly, N., Knight, M.R., Thuleau, P., Graziana, A., Muto, S., Ranjeva, R., and Mazars, C. (2001). The nucleus together with the cytosol generates patterns of specific cellular calcium signatures in tobacco suspension culture cells. Cell Calcium *30*, 413–421.
16. Cessna, S.G., and Low, P.S. (2001). Activation of the oxidative burst in aequorin-transformed *Nicotiana tabacum* cells is mediated by protein kinase- and anion channel-dependent release of Ca^{2+} from internal stores. Planta *214*, 126–134.
17. Cessna, S.G., Chandra, S., and Low, P.S. (1998). Hypo-osmotic shock of tobacco cells stimulates Ca^{2+} fluxes deriving first from external and then internal Ca^{2+} stores. J. Biol. Chem. *273*, 27286–27291.
18. Kurusu, T., Nishikawa, D., Yamazaki, Y., Gotoh, M., Nakano, M., Hamada, H., Yamanaka, T., Iida, K., Nakagawa, Y., Saji, H., et al. (2012). Plasma membrane protein OsMCA1 is involved in regulation of hypo-osmotic shock-induced Ca^{2+} influx and modulates generation of reactive oxygen species in cultured rice cells. BMC Plant Biol. *12*, 11.
19. Kurusu, T., Yamanaka, T., Nakano, M., Takiguchi, A., Ogasawara, Y., Hayashi, T., Iida, K., Hanamata, S., Shinozaki, K., Iida, H., and Kuchitsu, K. (2012). Involvement of the putative Ca^{2+}-permeable mechanosensitive channels, NtMCA1 and NtMCA2, in Ca^{2+} uptake, Ca^{2+}-dependent cell proliferation and mechanical stress-induced gene expression in tobacco (Nicotiana tabacum) BY-2 cells. J. Plant Res. *125*, 555–568.
20. Hayashi, T., Harada, A., Sakai, T., and Takagi, S. (2006). Ca^{2+} transient induced by extracellular changes in osmotic pressure in Arabidopsis leaves: differential involvement of cell wall-plasma membrane adhesion. Plant Cell Environ. *29*, 661–672.
21. Shih, H.-W., Miller, N.D., Dai, C., Spalding, E.P., and Monshausen, G.B. (2014). The receptor-like kinase FERONIA is required for mechanical signal transduction in Arabidopsis seedlings. Curr. Biol. *24*, 1887–1892.
22. Yahraus, T., Chandra, S., Legendre, L., and Low, P.S. (1995). Evidence for a mechanically induced oxidative burst. Plant Physiol. *109*, 1259–1266.
23. Rouet, M.-A., Mathieu, Y., Barbier-Brygoo, H., and Laurière, C. (2006). Characterization of active oxygen-producing proteins in response to hypo-osmolarity in tobacco and Arabidopsis cell suspensions: identification of a cell wall peroxidase. J. Exp. Bot. *57*, 1323–1332.
24. Beffagna, N., Buffoli, B., and Busi, C. (2005). Modulation of reactive oxygen species production during osmotic stress in *Arabidopsis thaliana* cultured cells: involvement of the plasma membrane Ca^{2+}-ATPase and H^{+}-ATPase. Plant Cell Physiol. *46*, 1326–1339.
25. Takahashi, K., Isobe, M., and Muto, S. (1997). An increase in cytosolic calcium ion concentration precedes hypoosmotic shock-induced activation of protein kinases in tobacco suspension culture cells. FEBS Lett. *401*, 202–206.
26. Felix, G., Regenass, M., and Boller, T. (2000). Sensing of osmotic pressure changes in tomato cells. Plant Physiol. *124*, 1169–1180.
27. Tsugama, D., Liu, S., and Takano, T. (2012). A bZIP protein, VIP1, is a regulator of osmosensory signaling in Arabidopsis. Plant Physiol. *159*, 144–155.
28. Ludwig, A.A., Saitoh, H., Felix, G., Freymark, G., Miersch, O., Wasternack, C., Boller, T., Jones, J.D.G., and Romeis, T. (2005). Ethylene-mediated cross-talk between calcium-dependent protein kinase and MAPK signaling controls stress responses in plants. Proc. Natl. Acad. Sci. USA *102*, 10736–10741.
29. Liu, W., Fairbairn, D.J., Reid, R.J., and Schachtman, D.P. (2001). Characterization of two HKT1 homologues from Eucalyptus camaldulensis that display intrinsic osmosensing capability. Plant Physiol. *127*, 283–294.
30. Tsugama, D., Liu, S., and Takano, T. (2016). The bZIP protein VIP1 is involved in touch responses in Arabidopsis roots. Plant Physiol. *171*, 1355–1365.
31. Tsugama, D., Liu, S., and Takano, T. (2014). Analysis of functions of VIP1 and its close homologs in osmosensory responses of *Arabidopsis thaliana*. PLoS ONE *9*, e103930.
32. Haswell, E.S., and Verslues, P.E. (2015). The ongoing search for the molecular basis of plant osmosensing. J. Gen. Physiol. *145*, 389–394.
33. Le Roux, A.-L., Quiroga, X., Walani, N., Arroyo, M., and Roca-Cusachs, P. (2019). The plasma membrane as a mechanochemical transducer. Philos. Trans. R. Soc. Lond. B Biol. Sci. *374*, 20180221.
34. Gigli-Bisceglia, N., Engelsdorf, T., and Hamann, T. (2019). Plant cell wall integrity maintenance in model plants and crop species-relevant cell wall components and underlying guiding principles. Cell. Mol. Life Sci. Published online November 28, 2019. https://doi.org/10.1007/s00018-019-03388-8.
35. Cuevas-Velazquez, C.L., and Dinneny, J.R. (2018). Organization out of disorder: liquid-liquid phase separation in plants. Curr. Opin. Plant Biol. *45* (Pt A), 68–74.
36. Kobayashi, M., Miyamoto, M., Matoh, T., Kitajima, S., Hanano, S., Sumerta, I.N., Narise, T., Suzuki, H., Sakurai, N., and Shibata, D. (2018). Mechanism underlying rapid responses to boron deprivation in Arabidopsis roots. Soil Sci. Plant Nutr. *64*, 106–115.
37. Ranade, S.S., Syeda, R., and Patapoutian, A. (2015). Mechanically activated ion channels. Neuron *87*, 1162–1179.
38. Martinac, B. (2012). Mechanosensitive ion channels: an evolutionary and scientific tour de force in mechanobiology. Channels (Austin) *6*, 211–213.
39. Basu, D., and Haswell, E.S. (2017). Plant mechanosensitive ion channels: an ocean of possibilities. Curr. Opin. Plant Biol. *40*, 43–48.
40. Engelsdorf, T., Gigli-Bisceglia, N., Veerabagu, M., McKenna, J.F., Vaahtera, L., Augstein, F., Van der Does, D., Zipfel, C., and Hamann, T. (2018). The plant cell wall integrity maintenance and immune signaling systems cooperate to control stress responses in Arabidopsis thaliana. Sci. Signal. *11*, eaao3070.
41. Denness, L., McKenna, J.F., Segonzac, C., Wormit, A., Madhou, P., Bennett, M., Mansfield, J., Zipfel, C., and Hamann, T. (2011). Cell wall damage-induced lignin biosynthesis is regulated by a reactive oxygen species- and jasmonic acid-dependent process in Arabidopsis. Plant Physiol. *156*, 1364–1374.
42. Wormit, A., Butt, S.M., Chairam, I., McKenna, J.F., Nunes-Nesi, A., Kjaer, L., O'Donnelly, K., Fernie, A.R., Woscholski, R., Barter, M.C.L., and Hamann, T. (2012). Osmosensitive changes of carbohydrate metabolism

in response to cellulose biosynthesis inhibition. Plant Physiol. *159*, 105–117.

43. Haswell, E.S., and Meyerowitz, E.M. (2006). MscS-like proteins control plastid size and shape in *Arabidopsis thaliana*. Curr. Biol. *16*, 1–11.
44. Veley, K.M., Marshburn, S., Clure, C.E., and Haswell, E.S. (2012). Mechanosensitive channels protect plastids from hypoosmotic stress during normal plant growth. Curr. Biol. *22*, 408–413.
45. Hamilton, E.S., Jensen, G.S., Maksaev, G., Katims, A., Sherp, A.M., and Haswell, E.S. (2015). Mechanosensitive channel MSL8 regulates osmotic forces during pollen hydration and germination. Science *350*, 438–441.
46. Haswell, E.S., Peyronnet, R., Barbier-Brygoo, H., Meyerowitz, E.M., and Frachisse, J.M. (2008). Two MscS homologs provide mechanosensitive channel activities in the Arabidopsis root. Curr. Biol. *18*, 730–734.
47. Maksaev, G., and Haswell, E.S. (2012). MscS-like10 is a stretch-activated ion channel from *Arabidopsis thaliana* with a preference for anions. Proc. Natl. Acad. Sci. USA *109*, 19015–19020.
48. Zou, Y., Chintamanani, S., He, P., Fukushige, H., Yu, L., Shao, M., Zhu, L., Hildebrand, D.F., Tang, X., and Zhou, J.-M. (2016). A gain-of-function mutation in Msl10 triggers cell death and wound-induced hyperaccumulation of jasmonic acid in Arabidopsis. J. Integr. Plant Biol. *58*, 600–609.
49. Laubinger, S., Zeller, G., Henz, S.R., Sachsenberg, T., Widmer, C.K., Naouar, N., Vuylsteke, M., Schölkopf, B., Rätsch, G., and Weigel, D. (2008). At-TAX: a whole genome tiling array resource for developmental expression analysis and transcript identification in *Arabidopsis thaliana*. Genome Biol. *9*, R112.
50. Winter, D., Vinegar, B., Nahal, H., Ammar, R., Wilson, G.V., and Provart, N.J. (2007). An "electronic fluorescent pictograph" browser for exploring and analyzing large-scale biological data sets. PLoS ONE *2*, e718.
51. Veley, K.M., Maksaev, G., Frick, E.M., January, E., Kloepper, S.C., and Haswell, E.S. (2014). Arabidopsis MSL10 has a regulated cell death signaling activity that is separable from its mechanosensitive ion channel activity. Plant Cell *26*, 3115–3131.
52. Basu, D., Shoots, J.M., and Haswell, E.S. (2020). Interactions between the N- and C- termini of mechanosensitive ion channel *At*MSL10 are consistent with a three-step mechanism for activation. J. Exp. Bot. Published online April 13, 2020.
53. Tateno, M., Brabham, C., and DeBolt, S. (2016). Cellulose biosynthesis inhibitors - a multifunctional toolbox. J. Exp. Bot. *67*, 533–542.
54. Zhu, X., Feng, Y., Liang, G., Liu, N., and Zhu, J.-K. (2013). Aequorin-based luminescence imaging reveals stimulus- and tissue-specific Ca^{2+} dynamics in Arabidopsis plants. Mol. Plant *6*, 444–455.
55. Knight, M.R., Campbell, A.K., Smith, S.M., and Trewavas, A.J. (1991). Transgenic plant aequorin reports the effects of touch and cold-shock and elicitors on cytoplasmic calcium. Nature *352*, 524–526.
56. Petrov, V., Hille, J., Mueller-Roeber, B., and Gechev, T.S. (2015). ROS-mediated abiotic stress-induced programmed cell death in plants. Front. Plant Sci. *6*, 69.
57. Locato, V., Paradiso, A., Sabetta, W., De Gara, L., and de Pinto, M.C. (2016). Nitric oxide and reactive oxygen species in PCD signaling. In Advances in Botanical Research: Nitric Oxide and Signaling in Plants, D. Wendehenne, ed. (Academic), pp. 165–192.
58. Bolwell, G.P., and Wojtaszek, P. (1997). Mechanisms for the generation of reactive oxygen species in plant defence – a broad perspective. Physiol. Mol. Plant Pathol. *51*, 347–366.
59. Dunand, C., Crèvecoeur, M., and Penel, C. (2007). Distribution of superoxide and hydrogen peroxide in Arabidopsis root and their influence on root development: possible interaction with peroxidases. New Phytol. *174*, 332–341.
60. Jiang, K., Schwarzer, C., Lally, E., Zhang, S., Ruzin, S., Machen, T., Remington, S.J., and Feldman, L. (2006). Expression and characterization of a redox-sensing green fluorescent protein (reduction-oxidation-sensitive green fluorescent protein) in Arabidopsis. Plant Physiol. *141*, 397–403.
61. van Doorn, W.G. (2011). Classes of programmed cell death in plants, compared to those in animals. J. Exp. Bot. *62*, 4749–4761.
62. Olvera-Carrillo, Y., Van Bel, M., Van Hautegem, T., Fendrych, M., Huysmans, M., Simaskova, M., van Durme, M., Buscaill, P., Rivas, S., Coll, N.S., et al. (2015). A conserved core of programmed cell death indicator genes discriminates developmentally and environmentally induced programmed cell death in plants. Plant Physiol. *169*, 2684–2699.
63. Huysmans, M., Lema A, S., Coll, N.S., and Nowack, M.K. (2017). Dying two deaths - programmed cell death regulation in development and disease. Curr. Opin. Plant Biol. *35*, 37–44.
64. Kumar, S.R., Mohanapriya, G., and Sathishkumar, R. (2016). Abiotic stress-induced redox changes and programmed cell death in plants—a path to survival or death? In Redox State as a Central Regulator of Plant-Cell Stress Responses, D.K. Gupta, J.M. Palma, and F.J. Corpas, eds. (Springer International Publishing), pp. 233–252.
65. De Pinto, M.C., Locato, V., and De Gara, L. (2012). Redox regulation in plant programmed cell death. Plant Cell Environ. *35*, 234–244.
66. Tripathi, A.K., Pareek, A., and Singla-Pareek, S.L. (2017). TUNEL assay to assess extent of DNA fragmentation and programmed cell death in root cells under various stress conditions. Bio-protocol *7*, e2502.
67. Xu, Q., and Zhang, L. (2009). Plant caspase-like proteases in plant programmed cell death. Plant Signal. Behav. *4*, 902–904.
68. Ge, Y., Cai, Y.-M., Bonneau, L., Rotari, V., Danon, A., McKenzie, E.A., McLellan, H., Mach, L., and Gallois, P. (2016). Inhibition of cathepsin B by caspase-3 inhibitors blocks programmed cell death in Arabidopsis. Cell Death Differ. *23*, 1493–1501.
69. Danon, A., Rotari, V.I., Gordon, A., Mailhac, N., and Gallois, P. (2004). Ultraviolet-C overexposure induces programmed cell death in Arabidopsis, which is mediated by caspase-like activities and which can be suppressed by caspase inhibitors, p35 and defender against apoptotic death. J. Biol. Chem. *279*, 779–787.
70. Young, B., Wightman, R., Blanvillain, R., Purcel, S.B., and Gallois, P. (2010). pH-sensitivity of YFP provides an intracellular indicator of programmed cell death. Plant Methods *6*, 27.
71. Wilkins, K.A., Bosch, M., Haque, T., Teng, N., Poulter, N.S., and Franklin-Tong, V.E. (2015). Self-incompatibility-induced programmed cell death in field poppy pollen involves dramatic acidification of the incompatible pollen tube cytosol. Plant Physiol. *167*, 766–779.
72. Roberts, J.K., Callis, J., Jardetzky, O., Walbot, V., and Freeling, M. (1984). Cytoplasmic acidosis as a determinant of flooding intolerance in plants. Proc. Natl. Acad. Sci. USA *81*, 6029–6033.
73. Bassil, E., Krebs, M., Halperin, S., Schumacher, K., and Blumwald, E. (2013). Fluorescent dye based measurement of vacuolar pH and K+. Bio-protocol *3*, e810.
74. Watanabe, N., and Lam, E. (2011). Arabidopsis metacaspase 2d is a positive mediator of cell death induced during biotic and abiotic stresses. Plant J. *66*, 969–982.
75. Yao, S., Luo, S., Pan, C., Xiong, W., Xiao, D., Wang, A., Zhan, J., and He, L. (2020). Metacaspase MC_1 enhances aluminum-induced programmed cell death of root tip cells in Peanut. Plant Soil *448*, 479–494.
76. Coll, N.S., Smidler, A., Puigvert, M., Popa, C., Valls, M., and Dangl, J.L. (2014). The plant metacaspase AtMC1 in pathogen-triggered programmed cell death and aging: functional linkage with autophagy. Cell Death Differ. *21*, 1399–1408.
77. Huang, L., Zhang, H., Hong, Y., Liu, S., Li, D., and Song, F. (2015). Stress-responsive expression, subcellular localization and protein-protein interactions of the rice metacaspase family. Int. J. Mol. Sci. *16*, 16216–16241.
78. Cosgrove, D.J. (2018). Nanoscale structure, mechanics and growth of epidermal cell walls. Curr. Opin. Plant Biol. *46*, 77–86.
79. Bou Daher, F., Chen, Y., Bozorg, B., Clough, J., Jönsson, H., and Braybrook, S.A. (2018). Anisotropic growth is achieved through the additive mechanical effect of material anisotropy and elastic asymmetry. eLife *7*, e38161.

80. Duval, I., Brochu, V., Simard, M., Beaulieu, C., and Beaudoin, N. (2005). Thaxtomin A induces programmed cell death in *Arabidopsis thaliana* suspension-cultured cells. Planta *222*, 820–831.

81. Zhou, F., Emonet, A., Dénervaud Tendon, V., Marhavy, P., Wu, D., Lahaye, T., and Geldner, N. (2020). Co-incidence of damage and microbial patterns controls localized immune responses in roots. Cell *180*, 440–453.e18.

82. Oiwa, Y., Kitayama, K., Kobayashi, M., and Matoh, T. (2013). Boron deprivation immediately causes cell death in growing roots of *Arabidopsis thaliana* (L.) Heynh. Soil Sci. Plant Nutr. *59*, 621–627.

83. Chaudhary, A., Chen, X., Gao, J., Leśniewska, B., Hammerl, R., Dawid, C., and Schneitz, K. (2020). The Arabidopsis receptor kinase STRUBBELIG regulates the response to cellulose deficiency. PLoS Genet. *16*, e1008433.

84. Hamann, T., Bennett, M., Mansfield, J., and Somerville, C. (2009). Identification of cell-wall stress as a hexose-dependent and osmosensitive regulator of plant responses. Plant J. *57*, 1015–1026.

85. Raggi, S., Ferrarini, A., Delledonne, M., Dunand, C., Ranocha, P., De Lorenzo, G., Cervone, F., and Ferrari, S. (2015). The Arabidopsis class III peroxidase AtPRX71 negatively regulates growth under physiological conditions and in response to cell wall damage. Plant Physiol. *169*, 2513–2525.

86. Fusari, C.M., Kooke, R., Lauxmann, M.A., Annunziata, M.G., Enke, B., Hoehne, M., Krohn, N., Becker, F.F.M., Schlereth, A., Sulpice, R., et al. (2017). Genome-wide association mapping reveals that specific and pleiotropic regulatory mechanisms fine-tune central metabolism and growth in Arabidopsis. Plant Cell *29*, 2349–2373.

87. Stephan, A.B., Kunz, H.-H., Yang, E., and Schroeder, J.I. (2016). Rapid hyperosmotic-induced Ca2+ responses in Arabidopsis thaliana exhibit sensory potentiation and involvement of plastidial KEA transporters. Proc. Natl. Acad. Sci. USA *113*, E5242–E5249.

88. Van Moerkercke, A., Duncan, O., Zander, M., Šimura, J., Broda, M., Vanden Bossche, R., Lewsey, M.G., Lama, S., Singh, K.B., Ljung, K., et al. (2019). A MYC2/MYC3/MYC4-dependent transcription factor network regulates water spray-responsive gene expression and jasmonate levels. Proc. Natl. Acad. Sci. USA *116*, 23345–23356.

89. Marhava, P., Hoermayer, L., Yoshida, S., Marhavý, P., Benková, E., and Friml, J. (2019). Re-activation of stem cell pathways for pattern restoration in plant wound healing. Cell *177*, 957–969.e13.

90. Tran, D., Galletti, R., Neumann, E.D., Dubois, A., Sharif-Naeini, R., Geitmann, A., Frachisse, J.-M., Hamant, O., and Ingram, G.C. (2017). A mechanosensitive Ca^{2+} channel activity is dependent on the developmental regulator DEK1. Nat. Commun. *8*, 1009.

91. Guerringue, Y., Thomine, S., and Frachisse, J.M. (2018). Sensing and transducing forces in plants with MSL10 and DEK1 mechanosensors. FEBS Lett. *592*, 1968–1979.

92. Hedrich, R. (2012). Ion channels in plants. Physiol. Rev. *92*, 1777–1811.

93. Maksaev, G., Shoots, J.M., Ohri, S., and Haswell, E.S. (2018). Nonpolar residues in the presumptive pore-lining helix of mechanosensitive channel MSL10 influence channel behavior and establish a nonconducting function. Plant Direct *2*, e00059.

94. Coll, N.S., Epple, P., and Dangl, J.L. (2011). Programmed cell death in the plant immune system. Cell Death Differ. *18*, 1247–1256.

95. Mukhtar, M.S., McCormack, M.E., Argueso, C.T., and Pajerowska-Mukhtar, K.M. (2016). Pathogen tactics to manipulate plant cell death. Curr. Biol. *26*, R608–R619.

96. Huh, G.-H., Damsz, B., Matsumoto, T.K., Reddy, M.P., Rus, A.M., Ibeas, J.I., Narasimhan, M.L., Bressan, R.A., and Hasegawa, P.M. (2002). Salt causes ion disequilibrium-induced programmed cell death in yeast and plants. Plant J. *29*, 649–659.

97. Duan, Y., Zhang, W., Li, B., Wang, Y., Li, K., Sodmergen, Han, C., Zhang, Y., and Li, X. (2010). An endoplasmic reticulum response pathway mediates programmed cell death of root tip induced by water stress in Arabidopsis. New Phytol. *186*, 681–695.

98. Subbaiah, C.C., and Sachs, M.M. (2003). Molecular and cellular adaptations of maize to flooding stress. Ann. Bot. *91*, 119–127.

99. Locato, V., and De Gara, L. (2018). Programmed cell death in plants: an overview. In Plant Programmed Cell Death. Methods in Molecular Biology, L. Gara, and V. Locato, eds. (Humana), pp. 1–8.

100. Mehlmer, N., Parvin, N., Hurst, C.H., Knight, M.R., Teige, M., and Vothknecht, U.C. (2012). A toolset of aequorin expression vectors for in planta studies of subcellular calcium concentrations in *Arabidopsis thaliana*. J. Exp. Bot. *63*, 1751–1761.

101. Schindelin, J., Arganda-Carreras, I., Frise, E., Kaynig, V., Longair, M., Pietzsch, T., Preibisch, S., Rueden, C., Saalfeld, S., Schmid, B., et al. (2012). Fiji: an open-source platform for biological-image analysis. Nat. Methods *9*, 676–682.

102. Clough, S.J., and Bent, A.F. (1998). Floral dip: a simplified method for Agrobacterium-mediated transformation of *Arabidopsis thaliana*. Plant J. *16*, 735–743.

103. Edwards, K., Johnstone, C., and Thompson, C. (1991). A simple and rapid method for the preparation of plant genomic DNA for PCR analysis. Nucleic Acids Res. *19*, 1349.

104. Verslues, P.E., Agarwal, M., Katiyar-Agarwal, S., Zhu, J., and Zhu, J.-K. (2006). Methods and concepts in quantifying resistance to drought, salt and freezing, abiotic stresses that affect plant water status. Plant J. *45*, 523–539.

105. van der Weele, C.M., Spollen, W.G., Sharp, R.E., and Baskin, T.I. (2000). Growth of *Arabidopsis thaliana* seedlings under water deficit studied by control of water potential in nutrient-agar media. J. Exp. Bot. *51*, 1555–1562.

106. Kwon, Y., Shen, J., Lee, M.H., Geem, K.R., Jiang, L., and Hwang, I. (2018). AtCAP2 is crucial for lytic vacuole biogenesis during germination by positively regulating vacuolar protein trafficking. Proc. Natl. Acad. Sci USA *115*, E1675–E1683.

107. Kardash, E., Bandemer, J., and Raz, E. (2011). Imaging protein activity in live embryos using fluorescence resonance energy transfer biosensors. Nat. Protoc. *6*, 1835–1846.

108. Achard, P., Renou, J.-P., Berthomé, R., Harberd, N.P., and Genschik, P. (2008). Plant DELLAs restrain growth and promote survival of adversity by reducing the levels of reactive oxygen species. Curr. Biol. *18*, 656–660.

109. Chen, S.X., Yen, C.C., and Jiao, X.Z. (1996). Effect of osmotic shock on the redox system in plasma membrane of *Dunaliella salina*. Cell Res. *6*, 31–38.

110. Knight, H., Trewavas, A.J., and Knight, M.R. (1997). Calcium signalling in *Arabidopsis thaliana* responding to drought and salinity. Plant J. *12*, 1067–1078.

111. Tanaka, K., Choi, J., and Stacey, G. (2013). Aequorin luminescence-based functional calcium assay for heterotrimeric G-proteins in Arabidopsis. In Methods in Molecular Biology (Methods and Protocols, M.P. Running, ed. (Humana), pp. 45–54.

STAR★METHODS

KEY RESOURCES TABLE

REAGENT or RESOURCE	SOURCE	IDENTIFIER
Antibodies		
Living Colors A.v. Monoclonal Antibody (JL-8); anti-GFP	Takara Bio Clontech	Cat # 632380; RRID:AB_10013427
Goat Anti-Mouse IgG Antibody, HRP conjugate	Millipore-Sigma	Cat # 12-349; RRID:AB_390192
Monoclonal Mouse Anti-α-Tubulin antibody	Millipore-Sigma	Cat # T5168-100UL; RRID:AB_477579
Bacterial and Virus Strains		
Agrobacterium tumefaciens GV3101	Lab stock	N/A
Chemicals, Peptides, and Recombinant Proteins		
Murashige and Skoog Basal Salt Mixture	PhytoTechnology laboratories	Cat# M404
Agar, Micropropagation Grade	PhytoTechnology laboratories	Cat# A296
Triton X-100	Millipore-Sigma	Cat# T8787-100ML
MES-hydrate	Millipore-Sigma	Cat# M5287-50G
DTT	Millipore-Sigma	Cat# 43815-1G
KI	Millipore-Sigma	Cat# 221945-5G
DPI	Millipore-Sigma	Cat# D2926-10MG
SHAM	Millipore-Sigma	Cat# S607-5G
Hydrogen Peroxide (H_2O_2), 30% (Certified ACS)	Fisher Scientific	Cat#: H325-100
Phenylmethylsulfonyl fluoride (PMSF)	Millipore-Sigma	Cat# 10837091001
Dimethyl sulfoxide (DMSO)	Millipore-Sigma	Cat# D8418-50ML
Dexamethasone (DEX)	Millipore-Sigma	Cat#D4902
Isoxaben	Millipore-Sigma	Cat# 36138
DCB	Millipore-Sigma	Cat# D1068-10MG
PEG-8000	Sigma -Millipore	Cat# 6510-1KG
D-Mannitol	Sigma -Millipore	Cat# M4125-1KG
Bovine Serum Albumin lyophilized powder	Sigma -Millipore	Cat# A9418
Silwet L77	Lehle seeds	Cat# NC0628903
Proteinase K	Sigma -Millipore	Cat# 1245680500
Paraformaldehyde	Millipore-Sigma	Cat# 158127-500G
Protease Inhibitor Cocktail	Sigma -Millipore	Cat# P9599-1ML
Deoxyribonuclease I from bovine pancreas	Sigma -Millipore	Cat# D5025-15KU
Bovine Serum Albumin (BSA)	Sigma -Millipore	Cat#: A2153
Critical Commercial Assays		
M-MuLV Reverse Transcriptase	Promega	Cat# M1701
Evans blue	Millipore-Sigma	Cat# E2129-10G
dNTPs	New England Biolabs	Cat# N0447S
Gateway LR Clonase II Enzyme mix	Thermo Fisher	Cat# 11791100
RNeasy Plant Kit	QIAGEN	Cat# 74904
RNase-Free DNase Set	QIAGEN	Cat# 79254
SYBR Green PCR Master Mix	Thermo Fisher Scientific	Cat# 4364344
H_2DCFDA	Thermo Fisher Scientific	Cat# D399

(*Continued on next page*)

Continued

REAGENT or RESOURCE	SOURCE	IDENTIFIER
In Situ Cell Death Detection Kit, Fluorescein	Roche Applied Science	Cat# 11684795910
Click-it TUNEL Alexa 647	Thermo Fisher Scientific	Cat# C10247
BCECF, AM	Thermo Fisher Scientific	Cat# B1170
Coelenterazine, native	Millipore-Sigma	Cat# C2230-50UG
Pluronic F-127	Thermo Fisher Scientific	Cat# P3000MP
Caspase 3 Assay Kit, Fluorometric	Millipore-Sigma	Cat# CASP3F-1KT
DAPI	Millipore-Sigma	Cat# D9542-1MG
Citifluor Antifading Mounting Solutions	VWR	Cat# 100496-536
SuperSignal West Dura Detection Kit	Thermo Fisher Scientific	Cat# 34076
Quick Start Bradford Protein Assay	Bio-Rad	Cat# 500-0201
Experimental Models: Organisms/Strains		
Arabidopsis thaliana Col-0 wild-type	*Arabidopsis* Biological Resource Center	N/A
msl10-3G	[48]	N/A
msl10-1	[46]	*SALK_07625*
Arabidopsis thaliana Col-0; *35S:MSL10-GFP* (Line # *12-3*)	[51]	Transgenic Col-0
Arabidopsis thaliana Col-0; *35S:MSL10^{4D}-GFP* (Line # *6-15*)	[51]	Transgenic Col-0
msl10-1; MSL10g (Line # *1-2* and *5-1*)	[52]	Transgenic *msl10-1*
msl10-1; MSL10g^{7A} (Line # *21-1* and *13-6*)	[52]	Transgenic *msl10-1*
msl10-1; MSL10 g^{7D} (Line # *17-1* and *4-22*)	[52]	Transgenic *msl10-1*
Arabidopsis thaliana Col-0; *DEX::MSL10* (Line # *1-2* and *4-3*)	[52]	Transgenic Col-0
Arabidopsis thaliana Col-0; *DEX::MSL10^{4A}* (Line # *1-2* and *4-3*),	[52]	Transgenic Col-0
Arabidopsis thaliana Col-0; *DEX::MSL10^{4D}* (Line # *8-3* and *2-1*)	[52]	Transgenic Col-0
Arabidopsis thaliana Col-0; *UBI10::AQE-CYA* (Line # *13-3, 12-6* and *7-2*)	This paper	Transgenic Col-0
msl10-1; UBI10::AQE-CYA (Line # *3-12, 11-5* and *5-7*)	This paper	Transgenic *msl10-1*
msl10-3G; UBI10::AQE-CYA (Line # *1-2, 2-2* and *3-2*)	This paper	Transgenic *msl0-3G*
Arabidopsis thaliana Col-0; *35Sp::roGFP1*	This paper	Transgenic Col-0
msl10-1; 35Sp::roGFP1	This paper	Transgenic *msl10-1*
msl10-3G; 35Sp::roGFP1	This paper	Transgenic *msl0-3G*
Oligonucleotides		
For all oligonucleotides used for genotyping and cloning; See Table S1	Integrated DNA Technologies	N/A
Recombinant DNA		
35Sp::roGFP1	[60]	N/A
pBINU-CYA	[100]	N/A
Software and Algorithms		
Fiji-ImageJ	[101]	https://fiji.sc
Prism v7.0	GraphPad Software	http://www.graphpad.com
StepOne software v2.1	Thermo Fisher Scientific	https://downloads.thermofisher.com

(*Continued on next page*)

Continued

REAGENT or RESOURCE	SOURCE	IDENTIFIER
GeneSys image acquisition software	Syngene	https://www.syngene.com/
Adobe Illustrator Version 24.0.1	Adobe Systems Incorporated	https://www.adobe.com/products/illustrator.html
Adobe Photoshop Version 21.1.2	Adobe Systems Incorporated	https://www.adobe.com/products/photoshop.html
Olympus Fluoview FV3000 imaging software	Olympus Life Science	https://www.olympus-lifescience.com/
Other		
TECAN Pro200	TECAN	https://lifesciences.tecan.com/plate_readers/
Olympus DP80	Olympus Life Science	https://www.olympus-lifescience.com/
96-well microplates, white	Greiner Bio-One	Cat# 655075
96-well microplates, black	Greiner Bio-One	Cat# 655076
96-well microplates, clear	Greiner Bio-One	Cat# 651161
TaqI-v2, restriction enzyme	New England Biolabs	Cat# R0149L
Immobilon-P PVDF transfer membrane	EMD Millipore	Cat# IPVH00010

RESOURCE AVAILABILITY

Lead Contact

Further information and requests for resources and reagents should be directed to and will be fulfilled by the Lead Contact, Elizabeth S. Haswell (ehaswell@wustl.edu).

Materials Availability Statement

All materials generated in this study are available upon request.

Data and Code Availability

There is no dataset/code associated with this paper.

EXPERIMENTAL MODEL AND SUBJECT DETAILS

Plant materials

All *Arabidopsis thaliana* plants used in this study were in the Columbia-0 ecotype background. *msl10-3G* is *rea1*, an EMS-induced point mutant originally isolated as recessive gain-of-function mutant of *MSL10* [48]. T-DNA insertional mutant seeds of *msl10-1 (SALK_07625)* were obtained from the *Arabidopsis* Stock Centre [46]. Some transgenic lines used in this study were previously characterized, including *35S:MSL10-GFP* (line *12-3*), *35S:MSL10^{4D}-GFP* (line *6-15*) [51]; *DEX:MSL10* (line *1-2* and *4-3*), *DEX MSL10^{4A}* (line *1-4* and *4-2*) *DEX MSL10^{4D}* (line *8-3* and *2-1*), *MSL10 g (line 1-2* and *5-1)*, *MSL10 g^{7A}* (line*21-1* and *13-6*), and *MSL10 g^{7D}* (line *17-1* and *4-22*) [52]. Unless stated otherwise, all chemical reagents were obtained from Millipore-Sigma. Seeds were surface-sterilized with 50% (v/v) bleach for 5 min and washed five times with sterilized water before plating. *Arabidopsis* plants were germinated and grown on vertically oriented Petri plates containing culture medium (CM) (4.3g/L Murashige and Skoog basal salts, 0.5 g/L MES, pH 5.7) and 0.8% [w/v] agar for 3-7 d depending on the experiments. For conditional induction of *MSL10*, seedlings were incubated with 30 μM dexamethasone (stock made up in 100% ethanol) dissolved in culture media + 140 mM mannitol for 12 h.

Accession numbers

The accession numbers for the genes discussed in this article are: *MSL10* (At5G12080), *PDF1.2* (At5G44420), *PERX34* (At3g49120), *UBQ5* (At3g62250), *EF1α* (At5g60390), *MC1* (AT1G02170), *MC2* (AT4G25110), *MC9* (AT5G04200), *WRKY18* (AT4G31800), *TCH1* (AT5G37780), *TCH2* (AT5G37770), *TCH3* (AT2G41100), *BFN1* (AT1G11190), *RNS3* (AT1G26820), *TCH4* (AT5G57560).

METHOD DETAILS

Generation of transgenic plants

In all cases, transgenes were introduced into plants using the floral dip method [102]. For genotyping, genomic DNA was extracted from leaves as previously described [103]. Primers used for cloning and genotyping are listed in Table S1. Wild-type, *msl10-1* and

msl10-3G lines were transformed with *35Sp::roGFP1* [60] and positive transformants selected on solid culture medium supplemented with 50 mg/L hygromycin. T3 homozygous progenies were used for further studies.

To obtain transgenic lines expressing cytoplasmic Aequorin, wild-type, *msl10-1* and *msl10-3G* lines were transformed with the pBINU-CYA transgene [100]. Phosphinothricin-resistant primary transformants were screened for GFP fluorescence and three independent T3 transgenic lines from each genetic background were used for further analysis.

Dose-dependent sensitivity of mannitol and PEG on seed germination

Seeds were sterilized and plated on CM with full- or half-strength Murashige and Skoog basal salts supplemented with the indicated concentrations of mannitol (0-500 mM) and polyethylene glycol (PEG) 8000 (0 to −1.2 MPa) as described [104, 105]. Plates were stratified in darkness for 3 d at 4°C and transferred to a culture room set at 23°C with a continuous light intensity of 120 μmol/m^2/s (fluorescence). Germination percentages were determined after 5 d from the end of stratification.

Relative root elongation

The primary root length was measured after 7 d of growth in culture media supplemented with either mannitol (0 or 140 mM mannitol) or PEG (0 to −0.5 MPa). Plates were scanned using the Syngene PXi imagining system equipped with GeneSys image acquisition software, and root length was measured using ImageJ.

Cell swelling treatments

This assay was modified from [10]. Briefly, seedlings were vertically grown on CM plates supplemented with 140 mM mannitol or PEG (−0.5 MPa, 1.5% w/v) for 5-6 days post germination. Seedlings were then equilibrated in liquid culture media supplemented with 140 mM mannitol or PEG (−0.5 MPa) for 4 h in 12-welled plates with gentle shaking. Six seedlings were placed in each well containing 2 mL of media. Either ISX (600 nM) or DCB (500 nM) was added to the liquid media during equilibration. For hypo-osmotic treatments, the existing media was replaced by CM containing 600 nM ISX but without mannitol or PEG for 6 h and 12 h. For iso-osmotic treatments, the existing media was replaced by fresh CM supplemented with 140 mM mannitol or with PEG (−0.5 MPa) and either ISX or DCB was added. Plates or liquid media containing PEG contained only 1/2-strength Murashige and Skoog basal salts.

Evans blue quantification

Seedlings were treated with 0.25% (w/v) Evans blue for 15 min, washed thoroughly, and homogenized in 10% methanol and 0.03% SDS. Blue color was quantified in 96-well plates in a plate reader (Infinite 200 PRO [Tecan]) by measuring absorbance at 630 nm. Values were normalized to total protein determined using the Quick Start Bradford Protein Assay (Bio-Rad) following the manufacturer's instruction.

TUNEL assay

The terminal deoxynucleotidyl transferase-mediated dUTP nick-end labeling (TUNEL) reaction was used to analyze cell swelling-induced DNA fragmentation as described previously [66] with minor modifications. Fixation, permeabilization and washing steps were performed in 12-welled plates, and the labeling reaction and staining were performed in 1.5 mL microcentrifuge tubes. Both iso- and hypo-osmotically-treated 5-day-old seedlings were fixed in 4% paraformaldehyde in PBS, pH 7.4 for 24 h at 4°C, then washed with 100% ethanol for 10 min. After fixation, seedlings were transferred to 70% ethanol for at least 16 h at –4°C. Dehydrated seedlings were washed five times with PBS and permeabilized for 30 min at 37°C with 0.1% Triton X-100 in 100 mM sodium citrate buffer, pH 6. Next, seedlings were incubated in 10 mM Tris-Cl, pH 7.5 supplemented with 20 μg/mL proteinase K for 30 min at 37°C and washed five times with PBS. *In situ* nick-end labeling of nuclear DNA fragmentation was performed for 1 h in the dark at 37°C using the *In Situ* cell death detection kit (Roche Applied Science) according to the manufacturer's manual. For GFP-tagged overexpression lines, the Click-it TUNEL Alexa 647 kit (Thermofisher) was used, following the manufacturer's instruction. After the TUNEL reaction, seedlings were rinsed 3 times in PBS and counterstained with DAPI (2.5 μg/mL) for 30 min in the dark, then mounted in the anti-fading reagent Citifluor (VWR International). For each biological replicate, a negative control omitting the terminal-deoxynucleotidyl-transferase and a positive control (DNase I; 1 μg/mL) treatment were included. The total number of TUNEL-positive nuclei in the transition/elongation zone of the root was quantified by overlaying a DAPI-stained root image with a bright-field image of the same root. Only those TUNEL-stained nuclei that overlapped with DAPI signal were counted as positive. Data were reported as a percentage of DAPI-positive nuclei.

Caspase-3-like activity

Seedlings were harvested at the indicated time points after cell swelling and caspase-3-like activity measured by determining the cleavage of the fluorogenic caspase-3 substrate Ac-DEVD-AMC using a commercial kit (Caspase 3 Fluorometric Assay Kit, Millipore-Sigma). Briefly, seedlings were ground to a powder in liquid nitrogen with a mortar and pestle. The powder was collected in 1.5 mL tubes and resuspended in assay buffer (20% glycerol, 0.1% Triton, 10 mm EDTA, 3 mM dithiothreitol, 2 mM phenylmethylsulphonyl fluoride, and 50 mM sodium acetate, pH 7.4) as described [69]. Isolated cytoplasmic protein was incubated with acetyl-Asp-Glu-Val-Asp-7-amido-4-methyl coumarin or Ac-DEVD-AMC (50 μM final concentration) for 1 hour at room temperature in the dark. Release of fluorescent AMC was measured with a 360 nm excitation wavelength and 460 nm emission wavelength in a TECAN Pro200 plate reader. Known amounts of hydrolyzed AMC were used to generate a calibration curve following the manufacturer's

instruction. Caspase enzymatic activity was calculated by finding the slope of the product's concentration plotted as a function of time. This activity was then standardized to the quantity of total proteins present in the sample (Bradford assay, Bio-Rad). Some samples were resuspended in assay buffer and preincubated for 1 h with a caspase inhibitor (Ac-DEVD-CHO; 100 μM) before being subjected to the enzymatic assay described above.

Vacuolar pH

Vacuolar pH was measured as described [106] with minor modifications. 10 μM BCECF-AM and 0.02% (v/v) Pluronic F-127 (Invitrogen) in liquid CM containing 140 mM mannitol and 600 nM ISX was added to seedlings during the last hour of their equilibration, then they were incubated in the dark for 1 h with gentle shaking. Seedlings were washed twice with same media but without the dye, then subjected to iso-osmotic or hypo-osmotic treatment as described as described in Figure 1B for 3 hours. Florescence images of stained roots were obtained using a confocal microscope (Olympus Fluoview FV3000) with excitation at 445 and 488 nm and emission at 525–550 nm. Fluorescence intensity in the elongation zone of roots obtained at 488 nm excitation was divided by that obtained at 445 nm excitation using Fiji [101]. An *in situ* calibration was performed separately using wild-type seedlings to make a calibration curve as described by [106]. Relative changes in vacuolar pH were calculated using the calibration curve. Ratiometric images were generated as described previously [107].

Monitoring ROS

Accumulation of ROS was assayed by confocal microscopy of seedlings stained with the fluorescent dye 2′,7′-dichlorofluorescin diacetate (H_2DCFDA; Millipore-Sigma) as described previously [108]. Five-day-old seedlings were subjected to cell swelling as described in Figure 1B for either 30 min or 60 min. Seedlings were then collected and incubated in the dark with 50 μM H_2DCFDA dissolved in either CM supplemented with 140 mm mannitol or CM alone during the last 15 min of their treatment. Finally, H_2DCFDA-stained seedlings were washed three times with the appropriate medium before imaging. For the quantification of fluorescence, H_2DCFDA stained seedlings were excited at 488 nm; emitted light was detected at 505 to 530 nm. The green fluorescence in the elongation zone of roots was quantified using Fiji software [101]. Fluorescent pixel intensity was quantified after subtracting the pixel intensity of the background. Data are reported as relative fold change (fluorescence intensity of treated root)/ (fluorescence intensity of control root), to account for mechanical perturbations that occurred during the assay. For ROS inhibition, seedlings were incubated with ROS inhibitors or scavengers, including KI (10 μM), DPI (10 μM) and SHAM (50 μM) as previously described [18, 23, 109]. These chemicals were added during the 4-hour equilibration step before seedlings were subjected to iso- or hypo-osmotic treatments.

Measuring redox status using roGFP biosensors

For ratiometric analysis of roGFP1, seedlings expressing cytoplasmic roGFP1 were excited with 405 and 488 nm lasers, and emission was collected at 510 nm using a confocal laser scanning microscope (Olympus Fluoview FV 3000). Fluorescence intensity was determined from the transition/elongation zone of seedlings subjected to cell swelling treatments. The ratio of fluorescence obtained at 405 nm divided by that obtained at 488 nm was calculated using Fiji software [101]. To calibrate the roGFP1 probe, seedlings harboring roGFP1 were treated with 10 mM DTT (full reduction) or with 10 mM H_2O_2 (complete oxidation), as previously described [60].

Aequorin-based $[Ca^{2+}]_{cyt}$ luminescence

Three-day-old seedlings of wild-type, *msl10-1* and *msl10-3G* mutant lines expressing Aequorin (*AEQ*) were used for monitoring $[Ca^{2+}]_{cyt}$ as described [87]. Briefly, seedlings were transferred individually to wells of sterile, white, 96-well microplates (Greiner Bio-One) containing 130 μL of CM supplemented with 140 mM mannitol and 2 μM native coelenterazine (Millipore-Sigma) and incubated overnight in darkness and at room temperature. The following day, 600 nM ISX (1.3 μl) was added to each well and the plate gently shaken for 4 hours. In a plate reader, the baseline luminescence was measured for 5 s, then 150 μL of either water or 140 mM mannitol was injected to produce hypo-osmotic or iso-osmotic treatments, respectively. The injection speed was set at 150 μL^{s-1}. The luminescence emitted from the seedlings was measured for 30 s. Conversion of luminescent values to $[Ca^{2+}]_{cyt}$ was performed as described [110, 111]. Background signal from wild-type, *msl10-1*, or *msl10-3G* lines without *AEQ* was subtracted. In some cases, the *msl9-1* mutant allele was segregating in the *msl10-1* background, but we did not observe any difference in calcium response between siblings.

Gene expression analysis

RNA was extracted from seedlings subjected to cell swelling as described in Figure 1B using the RNeasy Plant Mini Kit with in-column DNase I digestion (QIAGEN). Five hundred ng total RNA was reverse transcribed using oligo(dT) and the MLV reverse transcription system (Promega) following the manufacturer's instructions. qRT-PCR was performed in 25 μL reaction volumes with gene-specific primers and conducted with a StepOne Plus Real-time PCR System (Applied Biosystems) using the SYBR Green qPCR Master Mix (Thermofisher) and data were processed by StepOne Software (v2.0.1). *ELONGATION FACTOR 1α* (*EF1α*) and *UBIQUITIN 10* (*UBQ10*) were used as reference genes for normalization of gene expression levels as previously described [52]. Reported expression levels were normalized to the wild-type at 0 h or control treatment as indicated in figure legends. Primer sequences are listed in Table S1.

Immunoblot analysis

Total protein extraction and immunoblotting was performed according to a method described previously [51, 52]. 12- to 18-day-old seedlings were collected in a 2 mL microcentrifuge tube, weighed, frozen in liquid nitrogen, homogenized with eppendorf-sized pestle in 2X sample buffer, and denatured for 10 min at 70°C. Protein samples were resolved by 10% SDS-PAGE and transferred to polyvinylidene difluoride membranes (Millipore) for 16 h at 100 mA. Transferred proteins were first probed with anti-GFP antibodies (Takara Bio, 1:5,000 dilution) for 16 h. Next, the membrane was re-probed with anti-tubulin antibodies (Millipore-Sigma, 1:20,000 dilution) for 2 h. In both cases, a 1 h incubation with horseradish peroxidase-conjugated anti-mouse secondary antibodies (1:10,000 dilution; Millipore) was performed. Detection was performed using the SuperSignal West Dura Detection Kit (Thermo Fisher Scientific).

QUANTIFICATION AND STATISTICAL ANALYSIS

The procedures for the quantification of cell death, cell size, gene expression, intracellular Ca^{2+} transients, ROS levels, TUNEL-positive nuclei, caspase 3-like activity, vacuolar pH, root length, and seed germination are described in the respective Method Details subsections. Graphing and statistical analysis was performed with GraphPad Prism version 7.04. In all cases, significant differences refer to statistical significance at $p \leq 0.05$. The specific statistics applied in each experiment are indicated in the corresponding figure legends. Figures were prepared using Adobe Photoshop (v 21.1.2) and Illustrator CC (Adobe v 24.0.1).